ME-TR-033-3

HEAT TRANSFER BETWEEN SURFACES IN CONTACT:

THE EFFECT OF LOW CONDUCTANCE INTERSTITIAL MATERIALS

PART III

COMPARISON OF THE EFFECTIVE THERMAL INSULATION FOR INTERSTITIAL MATERIALS UNDER COMPRESSIVE LOADS

by

P.A. Smuda and D.A. Gyorog

Research Sponsored by
AMES RESEARCH CENTER
NATIONAL AERONAUTICS AND SPACE ADMINISTRATION
under Grant NGR 03-001-033

Mechanical Engineering Department
Arizona State University
Tempe, Arizona

June, 1968

HEAT TRANSFER BETWEEN SURFACES IN CONTACT:
THE EFFECT OF LOW CONDUCTANCE INTERSTITIAL MATERIALS

PART III

COMPARISON OF THE EFFECTIVE THERMAL INSULATION FOR INTERSTITIAL MATERIALS UNDER COMPRESSIVE LOADS

by

P. A. Smuda and D. A. Gyorog

Research Sponsored by
Ames Research Center

NATIONAL AERONAUTICS AND SPACE ADMINISTRATION
under Grant NGR 03-001-033

Mechanical Engineering Department
Arizona State University
Tempe, Arizona

June, 1968

ACKNOWLEDGMENTS

The authors wish to express their appreciation to the National Aeronautics and Space Administration for financial support and to Ames Research Center for the loan of the test apparatus used in this study.

Special thanks and gratitude is also expressed to Joe Smith, Rod McIntire, Robert MacMillan, Frank Hombaker, Dick Fisher and Carlton Anderson for their exceptional help in the construction of the test facility and apparatus.

Acknowledgment is due to Dr. Fink of the United States Water Conservation Laboratory for his assistance in the vacuum weight measurement and to AiResearch Manufacturing Company of Arizona for assistance with surface roughness measurement.

Finally, appreciation is expressed to Leroy Fletcher for the assistance with the computer programs and especially to Shirley Lodwick for typing the manuscript.

TABLE OF CONTENTS

LIST OF TABLES

LIST OF FIGURES

NOMENCLATURE

A	Apparent area, sq ft
h	Thermal contact conductance, Btu/hr sq ft °F
I	Current, amps
k	Thermal conductivity, Btu/hr sq ft °F
L	Load, pounds
ℓ	Thickness, inches
P	Pressure, psi
Q	Heat transfer, Btu/hr
q	Heat flux, Btu/hr sq ft
R	Thermal contact resistance, hr sq ft°F/Btu
r	Resistance, ohms
T	Temperature, °F
ΔT	Junction temperature difference, °F
dt	Increment of temperature, °F
W	Weight, pounds
dx	Increment of length, inches
δ	Uncertainty increment
ρ	Density, lb/ft^3

Subscripts

0	Initial
a	Apparent
c	Per contact
e	Effective

j	Junction
ℓ	Heat loss

CHAPTER 1

INTRODUCTION

The effects of thermal contact conductance must be considered in many applications. For example, in the aerospace and semiconductor industries it is necessary to include the effect of thermal contact resistance in the design of various systems and components that are exposed to extreme temperature conditions. Also the thermal control design for spacecraft components, such as reflective and ablative shields, antenna struts, cryogenic storage compartments, and platform mounted heat sources, require a knowledge of the resistance to heat transfer between surfaces in contact.

The existence of contact conductance results in many problems in engineering applications. Nuclear fuel elements, aircraft joints, annealing rolled steel, etc., are a few examples of situations in which maximum heat transfer is desired. The restriction to heat transfer caused by the contact conductance could be diminished by increasing the pressure at the contact, provided the system components can withstand extreme mechanical loading, which may not be the case. However, it should be noted that thermal contact resistance can also be useful. Thermal isolation of spacecraft components, cryogenic storage compartments, etc., is enhanced by the existence of contact conductance.

In a recent paper by Thomas and Probert (26)*, it was pointed out that in the past few years several low temperature insulating systems of very high efficiency, i.e., "superinsulations", have been developed and that they were all marked by the distinct disadvantage of low mechanical strength. It was also noted that comparatively small compressive loads could irreversibly reduce the effective thermal resistivity of such materials by a factor of up to 100 with possible failure of the insulating system. A suggested approach to the problem was to make a thermal barrier out of layers of a material which had good mechanical and thermal properties, such as stainless steel. Experimentation indicated, however, that the insulating properties would depend on the thermal resistance of each interface and the number of interfaces.

The modes of heat transfer at the contacting surface are considered to be: 1) solid conduction through the true contact area; 2) gaseous, molecular, or other conduction through the interstitial fluid or filler; and 3) thermal radiation. The thermal contact conductance, h , is mathematically defined as

$$h = Q_j/A\Delta T$$

where Q_j is the heat transferred between the bounding surfaces of the contact gap, A is the apparent area of contact at the interface, and ΔT is defined temperature difference due to the presence of the interface. The thermal contact resistance, R , is defined as the

---

* Numbers in parentheses indicate references

reciprocal of hA. Historically, thermal contact conductance has been evaluated by experimentally determining the quantities of the right side of the above equation for a particular set of environmental conditions. The heat flux across the interface can be determined from either Fourier's equation of heat conduction or an energy balance on the test specimens. The apparent contact area is the surface area of the interface projected onto a plane perpendicular to the direction of the heat flow; however, this area usually differs markedly from the actual contact area, which is a function of surface roughness and waviness, and the load. The temperature drop across the interface is usually determined by either a linear or a curvilinear extrapolation of the specimen's axial temperature profile to the contacting surface.

Although many studies have been conducted on the subject of thermal contact resistance as indicated by the critical reviews of Hudack (18) and Minges (23), methods for accurate prediction of thermal conductances between contacting solids with and without interstitial materials have not been sufficiently established. The results of the previous investigations and comparative studies yielded several different theories, those of Cetinkale and Fishenden (6) and Laming (20), taking into consideration the effect of interstitial fluids. Only a very limited amount of data for the contact conductance of metallic joints with interstitial fillers is tabulated for ready use, and generally only trends are shown. Values presented are dispersed over a wide range of conditions, environmental conditions, and types of interstitial fillers and usually emphasize

the improvement of thermal contact conductance of a joint. The range of test and environmental conditions is illustrated by the experiments of Hargadon (16) and of Berman (3) which were conducted in Argon atmospheres at high specimen temperatures and in a vacuum with the specimens at cryogenic temperatures, respectively. A representative sample of the metallic specimens and interstitial materials used by these and other investigators is listed in Table 1.

TABLE I

PREVIOUS INVESTIGATIONS

Author		Metallic Specimen	Interstitial Material
Brunot and Buckland	(5)	AISI M27 Steel	Steel Shim (22 mil)
Weills and Ryder	(28)	SAE 4140 Steel AMS 4846 Bronze Aluminum	Texaco AEO-120 Oil
Dailey and Kaspareck	(9)	6061-T6 Aluminum AZ91C Magnesium Almag 35 Aluminum 356	Silicone Vacuum Grease Indium Foil Aluminum Foil
Cunnington	(8)	6061-T4 Aluminum AZ-31 Magnesium	Indium Foil Silicone Vacuum Grease Dow Corning DC-340
Jansson	(19)	Aluminum Beryllium	Epoxy Cement Indium Foil Lead Foil Aluminum Leaf Gold Leaf

TABLE I (Cont'd)

Fried and Costello	(13)	AZ-31 Magnesium 2024-T3 Aluminum	Lead Foil Aluminum Foil Copper Screen
Fried	(12)	2024-T-4 Aluminum 304 Stainless Beryllium AZ-31 Magnesium	Silicone Vacuum Grease Silicone Rubber
Cetinkale and Fishenden	(5)	Steel Brass Aluminum	Air Spindle Oil Glycerol
Barzelay	(2)	2024-T6 Aluminum 2024-T3 Aluminum Inconel X	Aluminum Sheet Brass Shim Asbestos Sheet Teflon Sheet Zinc Chromate Primer
Clausing and Chao	(7)	Brass AZ-31B Magnesium 303 Stainless 2024-T4 Aluminum	Silicone Vacuum Grease
Berman	(3)	Copper	Copper Disk (0.005 in) Steel Disk (0.001 in) Teflon Disk (0.012 in) Al_2O_3 Powder
Mikesell and Scott	(22)	Brass	Monel Disk (0.017) Stainless Steel 304 Disk (0.0195 in) Stainless Steel 302 Disk (0.0008 in) Pyrex-Glass Spheres (0.375 in dia.) Soda Lime Spheres (0.42 in. dia.) Ceramic Spheres (0.39 in dia.) Micarta Linen-Impregnated Spheres (0.375 in dia.)

TABLE I (Cont'd)

Thomas and Probert	(26)	Copper	"Staybrite" F.S.T. Stainless Steel "Speedicut 14" Tool Steel "Ever Ready" Stainless Steel Razor-Blade Blanks "Carp" Fabric Laminated Phenolic Resin Brass Shimstock

Some specific work with insulating materials for low temperature storage equipment was reported in 1956 by Mikesell and Scott (22). They conducted tests on two types of thermal insulating supports which could be used in cryogenic storage vessels: 1) non-metallic spheres (pyrex glass, sodalime, ceramic and micarta linen-impregnated), and 2) multiple-contact supports in the form of stacks of thin metallic plates or spirally wound strips. For an axial load of 300 pounds per sphere and mean junction temperature of 48°K, the pyrex glass spheres reduced the heat transfer at the junction to less than 0.17 Btu/hr per sphere. In contrast, the multiple layer column of metal sheets provided both good thermal and mechanical properties. For a column of 315 stainless steel 0.0008-inch-thick plates at 1000 psi and a mean temperature of 48°K, the thermal conduction was found to be only 2 percent of that of a solid conductor of the same dimensions. Later, Thomas and Probert (26) also considered multiple-layer insulations by conducting experiments on stacks of thin layers of stainless steel, tool steel, razor blade steel, phenolic laminate

and brass to determine the variations of thermal conductances with applied load. They found that the decrease in the contact conductance per unit area with reduction of contact pressure was more rapid than Holm's (17) prediction of the square root of the pressure. It was also noted that for their results the equivalent thermal conductivity of the test samples was proportional to the square root of the bulk thermal conductivity of the test materials.

As pointed out above and in a previous report (24) results on thermal conductance of metallic contacts with interstitial fillers are rather limited. The information which is available is dispersed over a wide range of interstitial fillers subjected to numerous test conditions with emphasis on the improvement of thermal contact conductance of a joint. However, only a few investigators (6, 8, 12, 13, 14, 19, 20, 22, 26) have tried to find ways of restricting heat flow between two surfaces in contact. Thus, there exists a need for additional information on low conductance interstitial materials for the purpose of designing insulated joints and of predicting the results for thermal isolation.

The primary objective of this investigation is to provide additional information on thermal contact resistance for the case of thermal barriers (insulators) inserted between plane parallel metal surfaces and to determine which of the tested materials are better. This is to be accomplished by the following procedure:

1. Comparative study of a number of interstitial fillers at varying pressures and temperatures.

2. Check runs on the better materials for repeatability.

3. Selection and more extensive study of the better insulating materials.

CHAPTER II

EXPERIMENTAL APPARATUS

The calculation of thermal contact conductance is directly dependent upon the determination of the heat flux at the junction and the resulting temperature difference across the junction. For an investigation of thermal contact conductance the apparatus should be flexible enough to subject the test samples to a wide range of environmental and physical conditions, but at the same time be sophisticated enough to insure accurate measurement of these conditions. The experiences and recommendations of many previous investigators such as Blum (4), Clausing and Chao (7), Fried (12) and Stubstad (25) were used in formulating the general specifications for the experimental facility. Since the interstitial materials were to be tested at vacuum conditions, an environmental pressure of 10^{-5} Torr was necessary in the vacuum test chamber. Also to yield a uniform heat flux at the specimen interface radiation shields were installed to minimize surface heat transfer and the length of the constant cross-sectional area of the specimens was selected to allow the temperature gradients in the metal specimens to become uniform. The capacities of the heat source and sink were chosen to obtain the temperature limits of approximately 500°F and -300°F, respectively. A range of load pressures from zero to 1000 psi was selected for the test conditions.

In addition it was desired to be able to vary the load on the test column or separate the specimens without releasing the vacuum. Instrumentation for measuring temperatures, vacuum pressure, energy input, and load pressure were also incorporated. Specific details of the design and construction of the test apparatus is available in two previous reports (11,24). However, for the purpose of clarity a general description is also presented in the following sections.

Vacuum Facility

A vacuum chamber, oil diffusion pump, mechanical forepump, chevron cooling baffle, high vacuum valves, and the necessary vacuum pressure measuring instruments composed the vacuum system. A schematic of the system is illustrated in Figure 1. The base plate was manufactured locally to fit the design specification for the test apparatus. To achieve the desired flexibility five universal feed throughs were installed in the base plate to seal passages for the test section support rods, the heater power input, the thermocouples, the high pressure nitrogen for the load bellows, and the heat sink coolant. Three vacuum valves were installed to isolate different regions of the vacuum system. These locations are indicated in Figure 1.

A schematic diagram of the water cooling system for the heat sink, chevron cooling baffle, and the diffusion pump is shown in Figure 2. As a safety precaution a power interlock was installed in the water line to prevent overheating in the case of a cooling

(1) Bell Jar
(2) Nitrogen Load Bellows Passthrough
(3) Passthrough Bellows
(4) Entry Gland
(5) High Vacuum Valve
(6) Water Cooling Baffle
(7) Oil Diffusion Pump
(8)(12)(14) Vacuum Thermocouple Gage
(9)(13) Vacuum Valves
(10) Ionization Gage
(11) Nitrogen Bleed Port
(15) Mechanical Pump

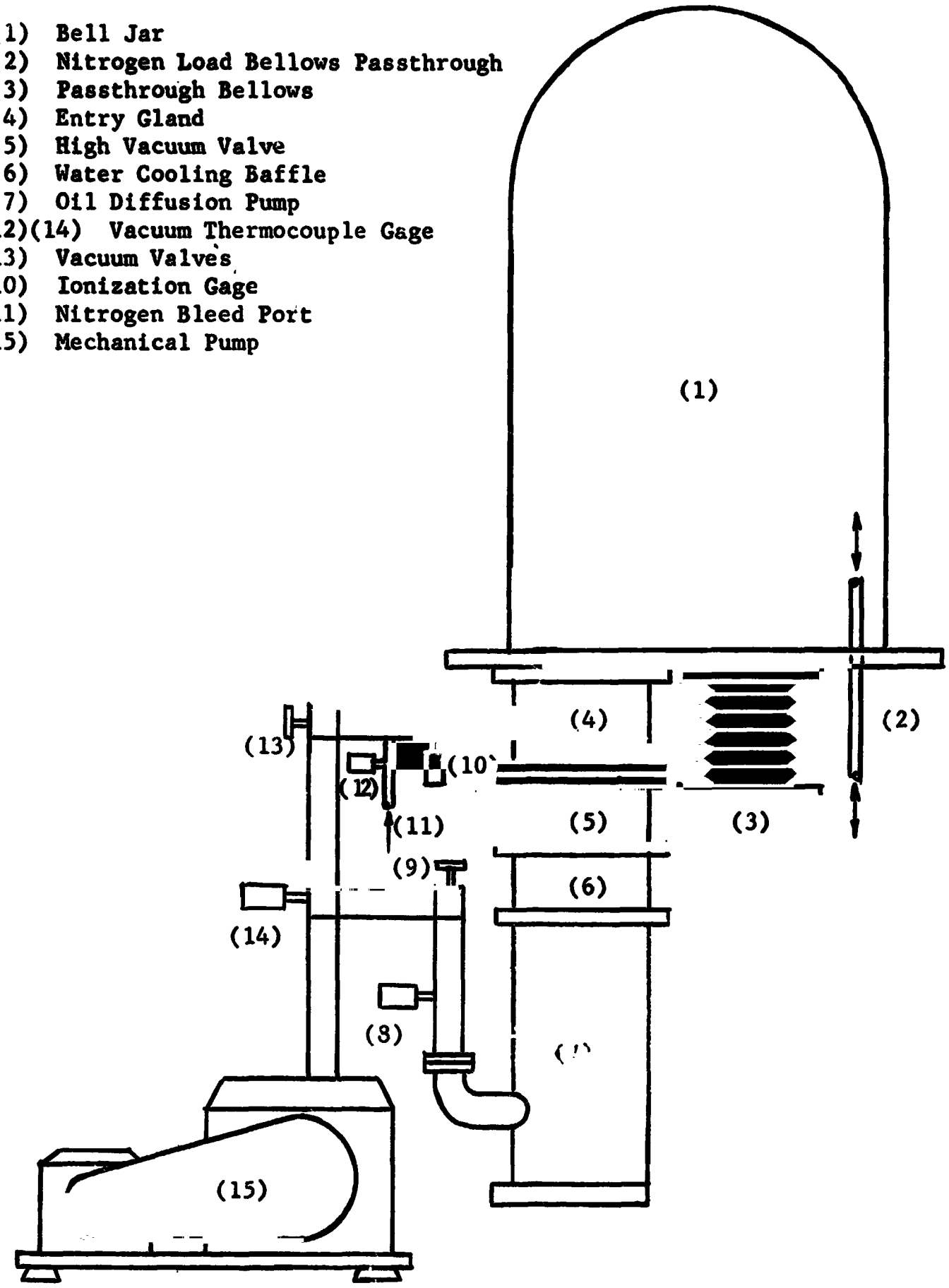

Figure 1. Schematic of the Vacuum System.

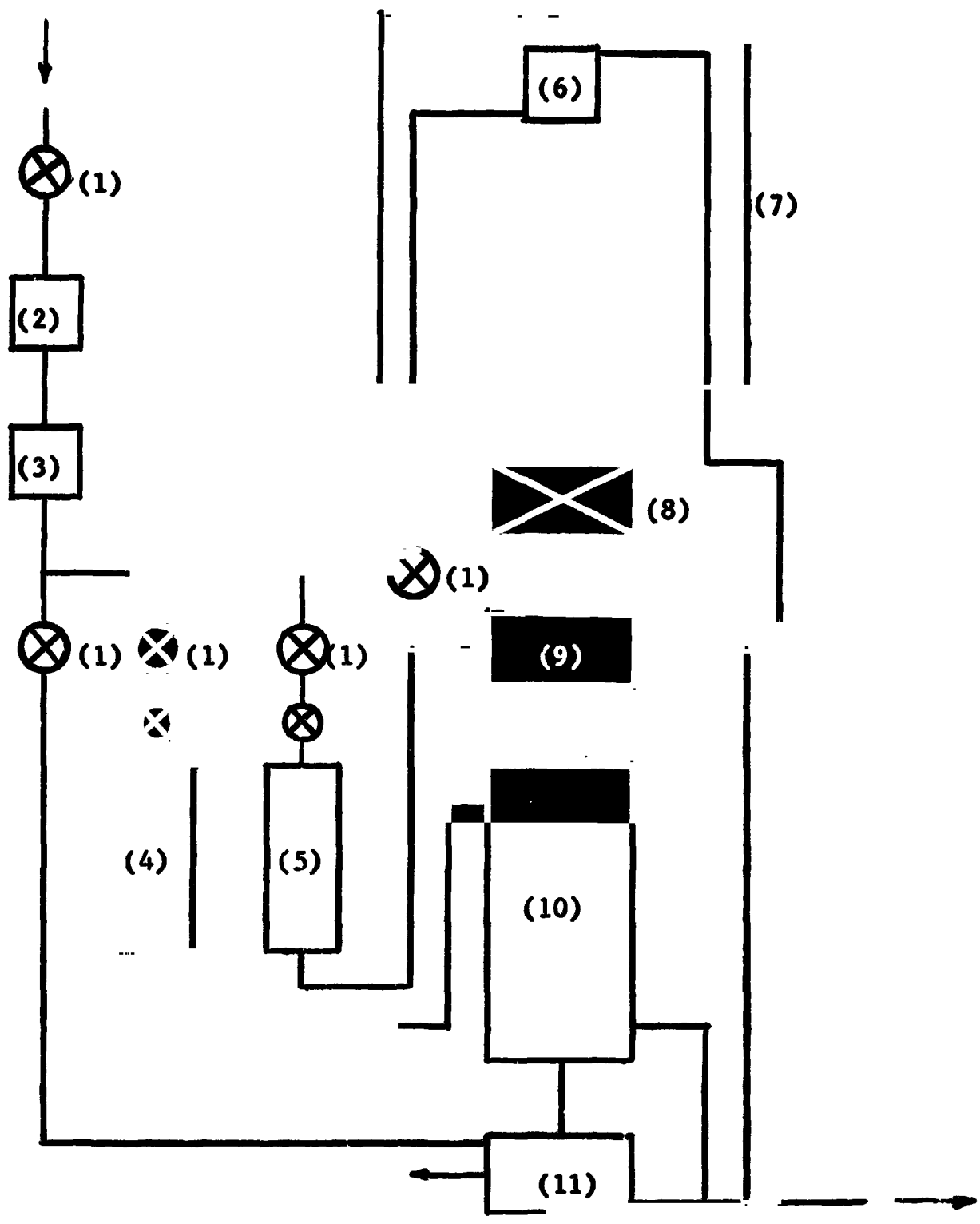

(1)	Water Valve	(7)	Vacuum Chamber
(2)	Water Filter	(8)	Vacuum Valve
(3)	Water Pressure-Power Interlock	(9)	Chevron Baffle
(4)(5)	Flowmeter	(10)	Diffusion Pump-Barrel
(6)	Heat Sink	(11)	Diffusion Pump-Forearm

Figure 2. Diagram of the Water Cooling System.

water loss. An NRC Model 507 ionization gage and three NRC Model 501 thermocouple gages were installed to monitor the vacuum system operation. The locations of these gages are also indicated in Figure 1. Throughout the test program vacuum pressures from 10^{-5} and 10^{-6} Torr were attained by the vacuum system.

Instrumentation

Since the calculation of the thermal contact conductance is largely dependent upon the temperature measurements, the accuracy of the thermocouples and thermocouple readout instrumentation is of major importance. The thermocouple circuits consisting of three thermocouple switches, copper-constantan 30 gage thermocouples, two potted thermocouple feed throughs, terminal strips in the vacuum chamber, ice junctions and the thermocouple potentiometer were calibrated. The uncertainty in the temperature measurement was estimated to be 0.5 percent (24).

After installing the instrumented specimens in the test apparatus, the thermocouple leads were attached to teflon strips. Each terminal supported twelve thermocouples and was fixed to the vertical support rods of the apparatus. The thermocouple leads from the passthrough were likewise attached to the terminal strip and were shielded from the heated and cooled portions of the test specimen to maintain isothermal conditions at the terminal junction. External to the vacuum chamber, the thermocouple leads were attached to bakelite terminal strips in a shielded region free from air currents. Leads were run from these connections to switches and

ice junctions through a grounded metal conduit. A reference junction was included in the circuit for each selector switch which in essence provided an individual cold junction for each thermocouple. The cold junction thermocouples were individually placed in small, oil-filled. glass tubes that were immersed in a distilled water and ice bath to provide a constant 32°F reference temperature. The thermocouple outputs were recorded with a Leeds and Northrup Model 8686 millivolt potentiometer. The smallest scale division on the potentiometer was 5 microvolts which represented 0.2°F for copper-constantan thermocouples for the range of temperatures considered. A schematic layout of the thermocouple system can be found on page 33 of Reference (24).

The apparent pressure on an interface is calculated by dividing the applied force on the specimens by the cross sectional area of the interface. The load force was measured with a BLH4 Model C3PI load cell, which was mounted on a mechanical screw jack below the vacuum chamber as shown in Figure 5, and a BL4 Model 120C strain indicator. To obtain the force actually applied to the interface, the measured load had to be corrected for the effect of the pass-through bellows and the weight of the test column. The force correction was determined by measuring the resisting force of the passthrough bellows as a function of the bellows deflection. The calibration results and techniques for the load measurement was discussed in Appendix B of Reference (24).

It was originally planned to control a.c. power input to the heater system with a variable transformer. The heater voltage and

current then could be measured with a voltmeter and an ammeter. However, later it was found to be necessary to calculate the interface heat transfer by an energy balance method. This required an accurate means of controlling and measuring the power input to the specimen. For this purpose a regulated filtered d.c. power supply was installed in series with the powerstat controlling the main heater. Voltage and current were measured with a potentiometer and with shunt arrangement shown in Figure 3. The uncertainties in these readings are estimated as 0.05 volts and 200 microamperes. Control of the guard heater power was obtained by adjusting a variable transformer.

Test Section

The test section was composed of the support frame, the test specimens, the source, the sink, the guard heater, the radiation shields, and the load mechanism (Figure 4). The test specimens were mounted in a stainless steel framework as shown in Figure 5. This particular construction prevented the force applied to the interface from being transmitted to the base plate. Thus, it was only necessary for the base plate to support the weight of the test section.

Design of the test specimens was a major consideration for several reasons. First, their size and shape dictated the dimensions for most of the other test section components. Second, the technique used to evaluate the thermal contact conductance required

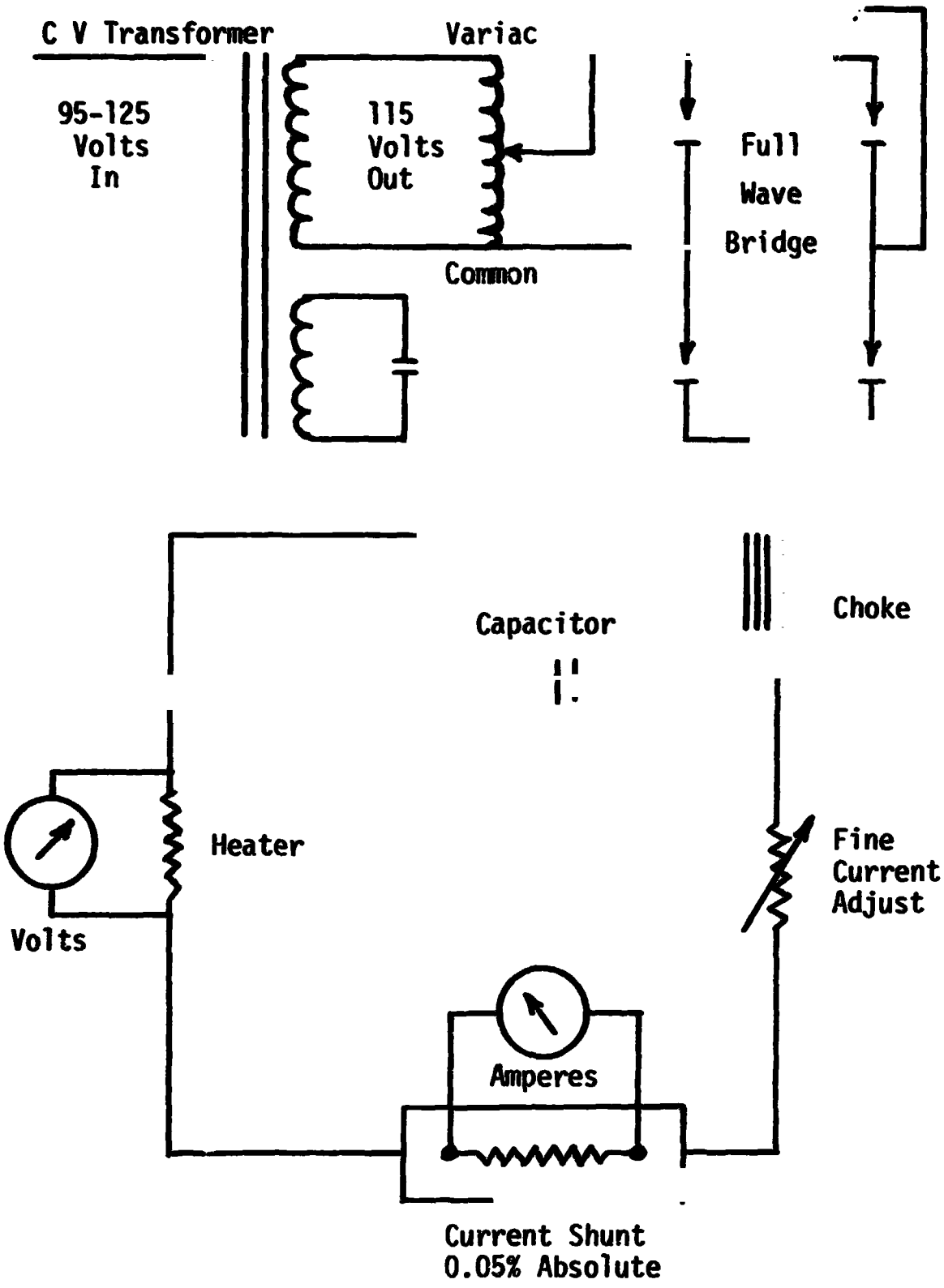

Note - Voltage and Current were measure with a potentiometer

1 volt = 1 millivolt
1 amp = 50 millivolts

FIGURE 3. Schematic of DC Power System

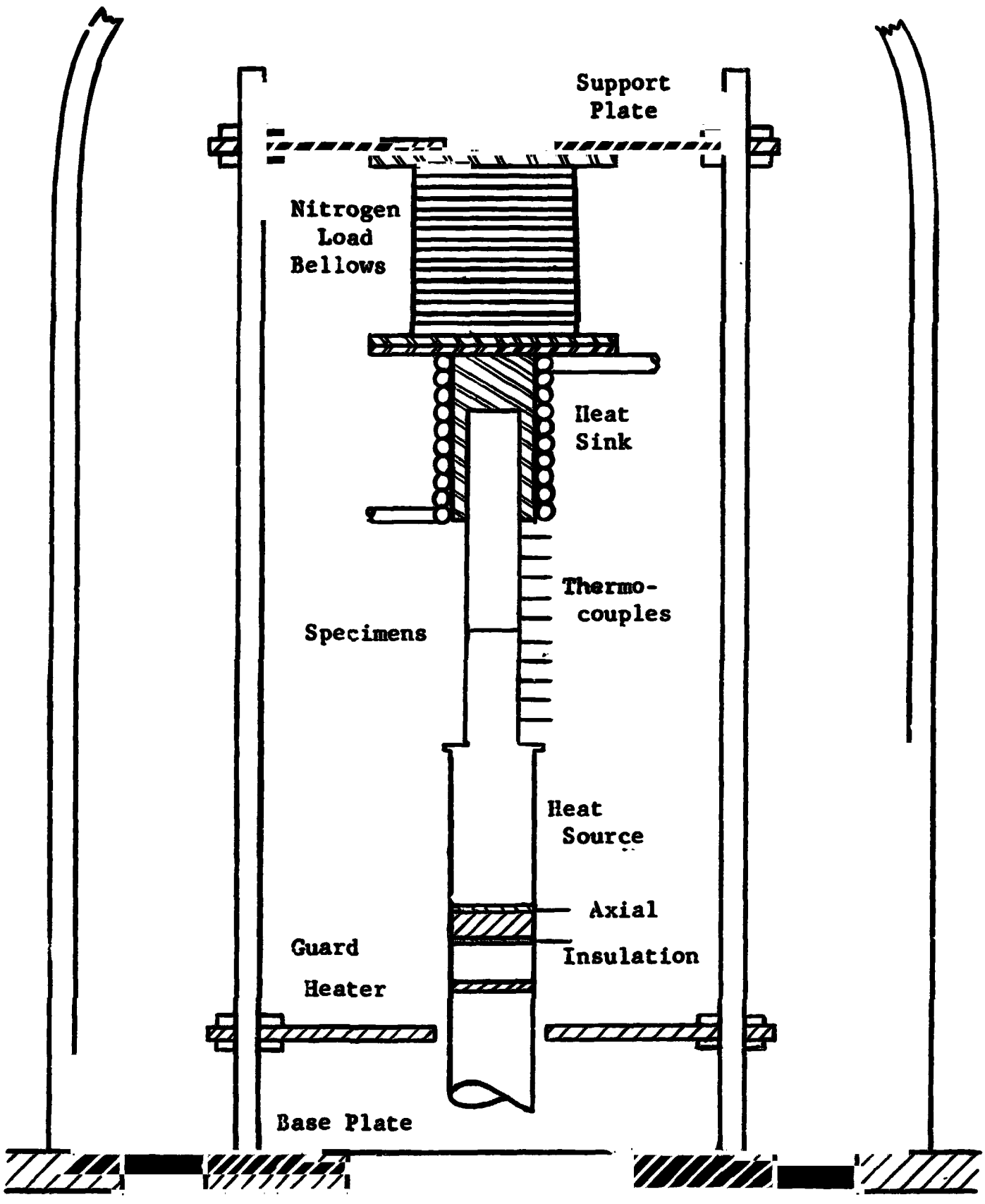

Figure 4, Schematic Diagram of the NASA Experimental Apparatus.

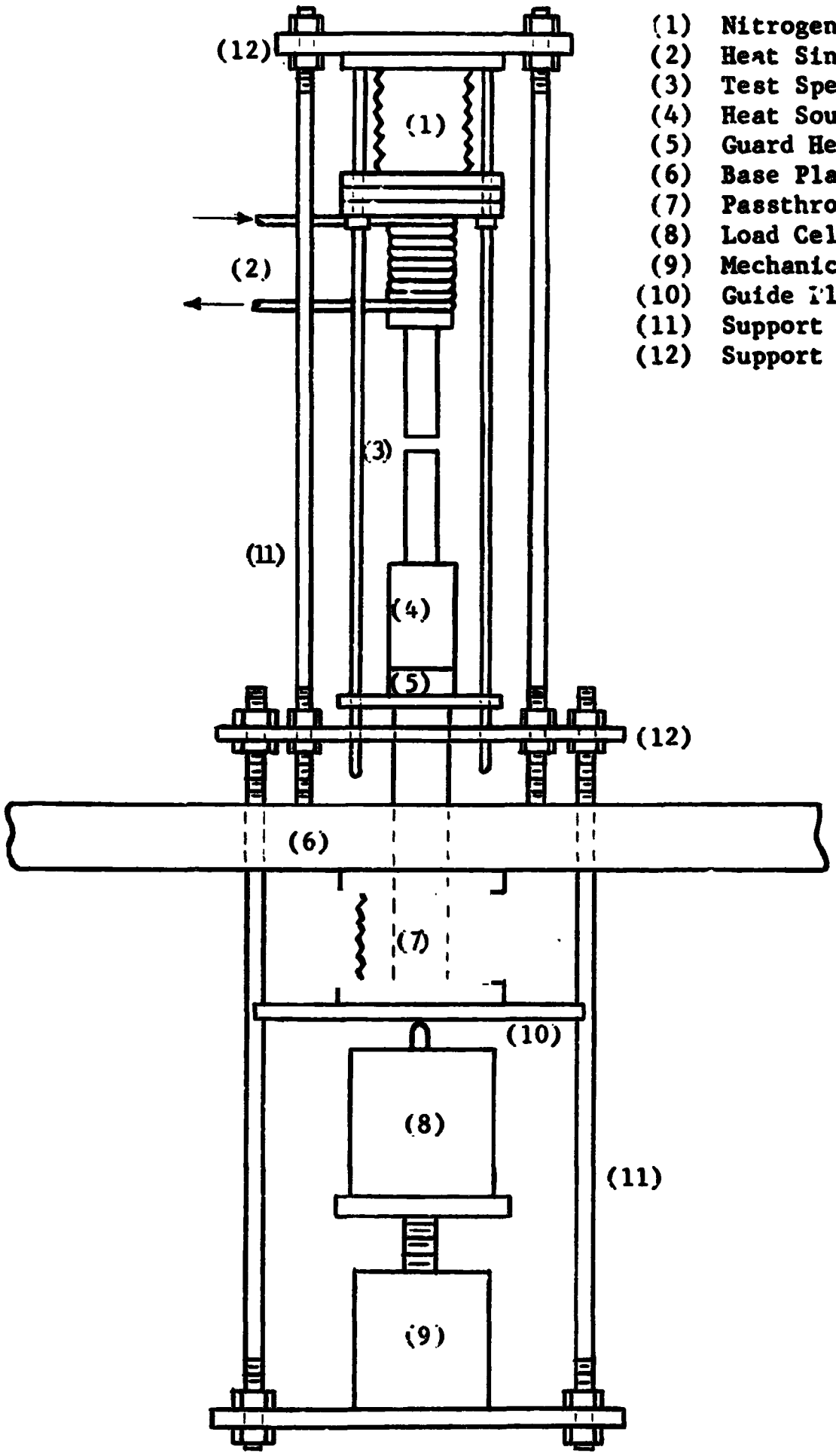

(1) Nitrogen Load Bellows
(2) Heat Sink
(3) Test Specimens
(4) Heat Source
(5) Guard Heater
(6) Base Plate
(7) Passthrough Bellows
(8) Load Cell
(9) Mechanical Screw-jack
(10) Guide Plate
(11) Support Rods
(12) Support Plate

Figure 5. Diagram of the Axial Loading System.

uniform heat flux above and below the interface. Finally, it was desirable to keep the geometry of the specimen as simple as possible to facilitate fabricating the relatively large number required.

A basic cylindrical configuration was specified for geometric simplicity. The heat metering portions of the metal specimens were one inch in diameter and two and one-half inches in length. Five centerline thermocouple holes were drilled at one-half inch increments starting at one-fourth inch from the interface edge. Three additional holes, one-sixteenth inch deep were drilled, diametrically opposed to the five holes, for measurement of surface temperatures. Detail drawings with the dimensions of the test specimens are presented in Figures 6 and 7.

Based on the temperature requirements a 300 watt Acrawatt BLOEF band heater was selected for the heat source. The heater element was one and one-half inches in diameter by three inches long and was capable of safely withstanding temperatures up to 600°F. The cooling element was constructed from a one and one-half inch diameter copper bar. A one-fourth inch copper cooling coil was attached to the external surface of the sink with silver solder and the metal test specimen was threaded into a one inch diameter hole centered in the copper bar. Cooling fluids such as water, steam, air, or liquid nitrogen can be used.

The heated test specimen was insulated axially and radially to minimize the heat losses. The radial insulation was PFW glass insulation loosely packed around the heater and held in place by a thin sheet of aluminum foil. To shield other components and further

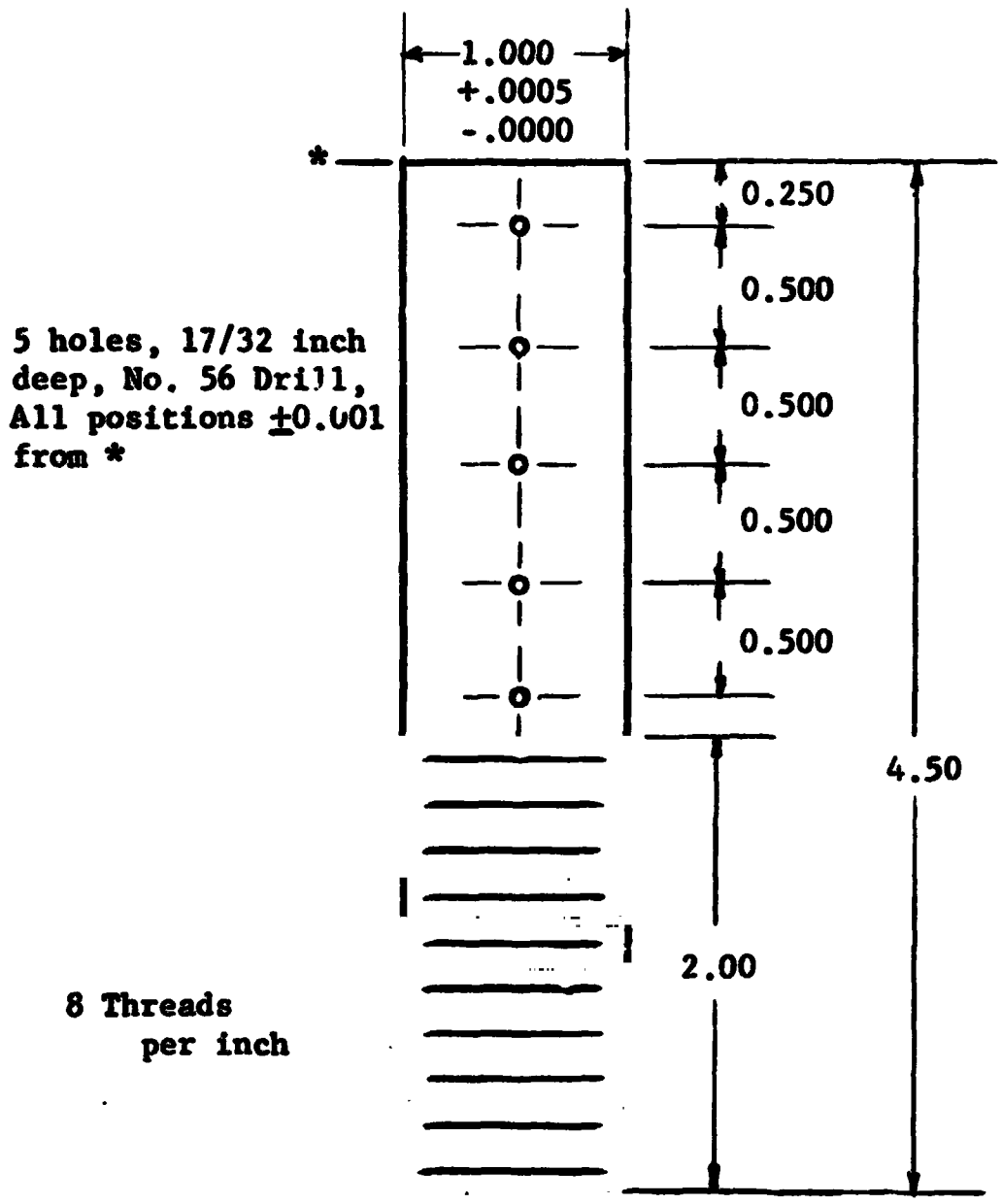

All dimensions in inches.

Figure 6. Details of the Sink Specimen.

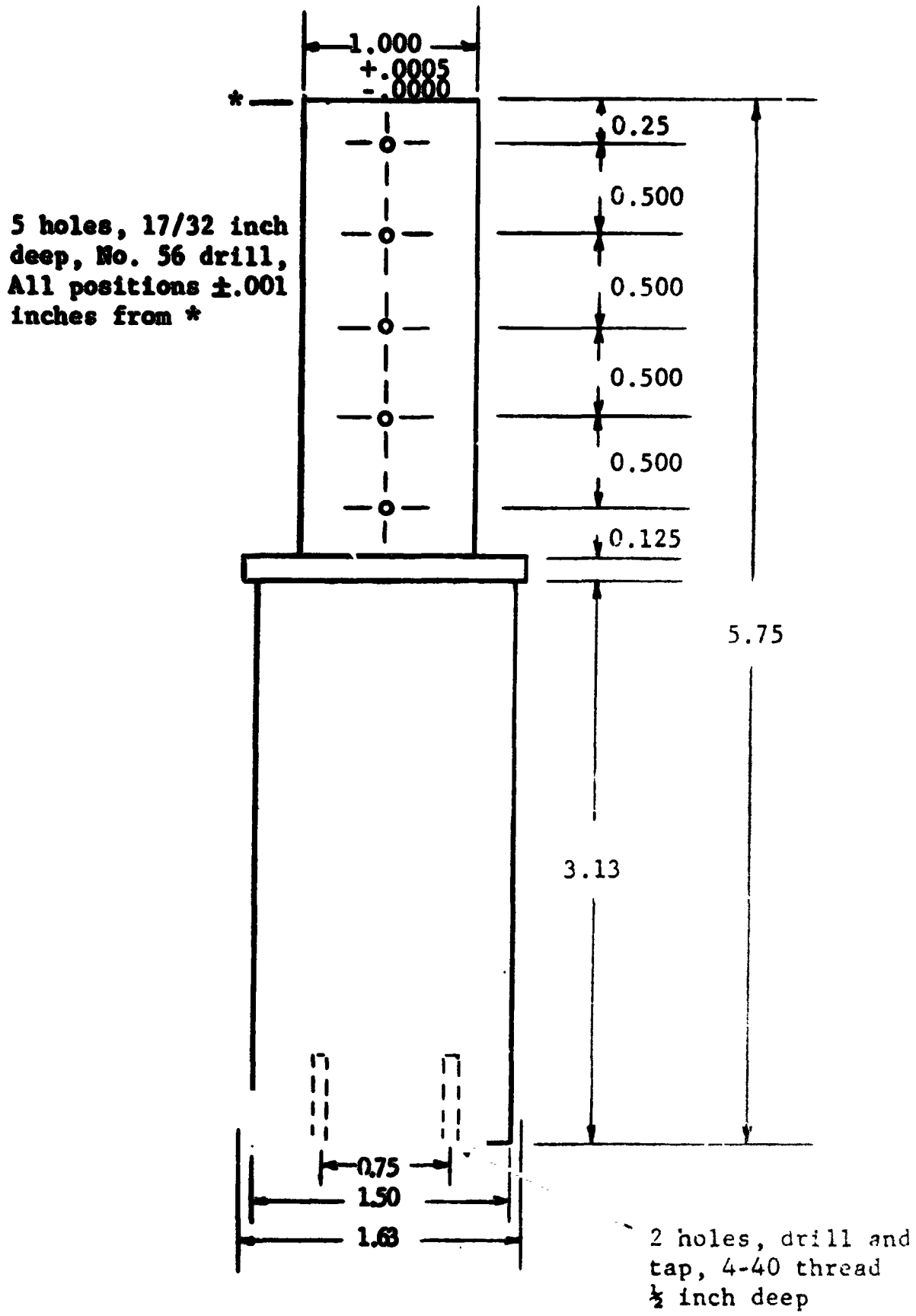

All dimensions in inches.

Figure 7. Details of the Source Specimen.

reduce the radial heat loss, an aluminum radiation shield was located about one inch away from the insulated heater. An aluminum cap was placed over the cylinder formed by this outer shield to prevent radiation to the instrumented section of the specimen. The axial insulator was formed from three layers of asbestos board sandwiched between two one-sixteenth inch thick aluminum disks. A guard heater located as shown in Figure 4 provided a more positive means of controlling the conduction heat losses along the specimen. This control was especially important for the energy balance calculation of the junction heat transfer.

Radiation shields were also installed to minimize the surface heat transfer from the instrumented sections of the test specimens. Several different shield configurations were tested. One such configuration was as follows:

> The heated specimen shield was constructed from WRP felt formed into a cylinder one and one-half inches in diameter and two and one-half inches in length. A layer of aluminum foil was secured to the inside surface of the cylinder. A split mica disk covered with aluminum foil and containing a one and one-quarter inch diameter hole was used to cover the top of the shield to insure complete enclosure of the heated specimen. The cooled specimen's shield was made from heavy duty aluminum foil formed into a cylinder one and one-half inches in diameter and two and one-half inches in length. Wire rolled into the edges of the foil was used to maintain the cylindrical shape of the shield and to provide

a means of attaching the shield to the cooler.

The results of the shield configuration test yielded the following conclusions:

1) Shields should be maintained as close as possible to the test specimens
2) They should cover the lengths of the specimens
3) Because of a large ΔT between the test specimens, a cold specimen shield connected to the sink and a hot specimen shield isolated from the heater are necessary to maintain a small temperature difference between the shields and specimens
4) Multiple shields only add complexity to the installation.

Thus, the final shield configuration used in this investigation was composed of two one and one-half inch in diameter aluminum foil cylinders two and one-half inches in length. The mounting procedure used was in accordance with statement three above.

The mechanical pressure applied to an interface has a major influence on the resulting thermal contact conductance. Therefore, the experimental apparatus had to incorporate a means of applying a variable load to the test junction, and adequate instrumentation to measure the load accurately. For load application to the test column a high pressure nitrogen gas bellows chamber and a Simplex Model J2 worm-gear screw jack were installed as integral parts of the test apparatus. The stainless steel bellows was designed for the pressures necessary to provide the required one thousand psi specimen loading. A diagram of the high pressure nitrogen system is

shown in Figure 8. The screw jack, located external to the vacuum chamber and below the passthroughs bellows, has a two ton capacity and a 15:1 gear ratio. Its purpose was to provide a means for raising and lowering the specimen. The three support rods below the base plate (Figure 5) also served to keep the passthrough bellcws and the interface in alignment.

The resulting experimental apparatus was tested over a temperature range of +300°F and -300°F with water and liquid nitrogen coolants, respectively, and a pressure range of zero to 1000 psi. Surface and centerline temperatures generally agreed within 0.5°F with a maximum difference within 2.0°F for the extreme temperature cases. The experimental values of thermal contact conductance determined with this apparatus were found to be repeatable and comparable to other published data.

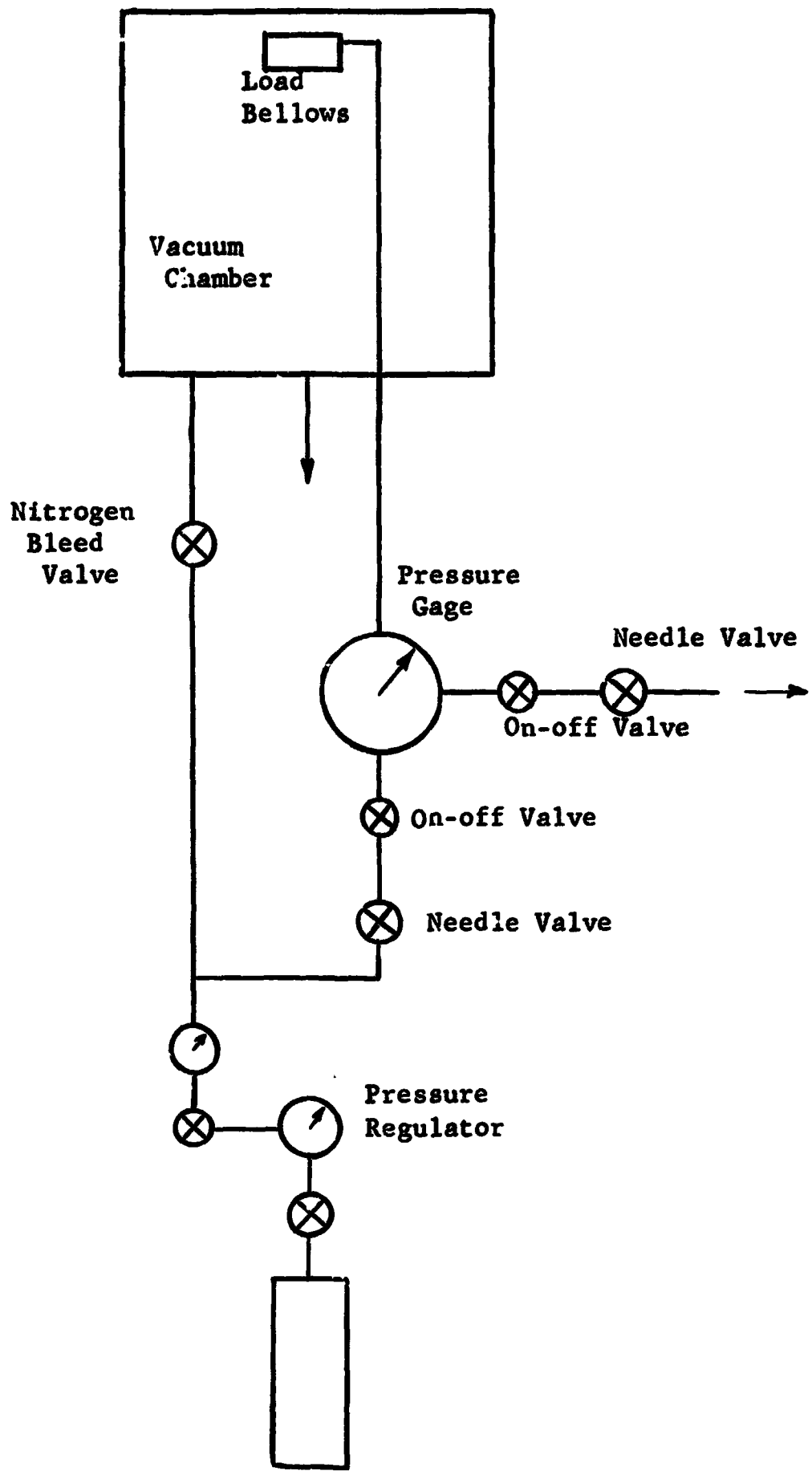

Figure 8. Diagram of the High Pressure Nitrogen System.

CHAPTER III

EXPERIMENTAL PROCEDURE AND TECHNIQUES

The experimental procedure was essentially the same for all tests. First the cylindrical metal specimens were installed and tested in a bare junction configuration and then a one inch diameter disc of the interstitial material was positioned between the metal specimens. The alignment of the test column during the evacuation of the test cell was maintained by a slight contact pressure. Once the desired vacuum level was obtained, the test conditions were set by adjusting; the nitrogen gas pressure in the load bellows, the power input to the main heater, and the coolant flow rate. The guard heater was monitored and adjusted to maintain a temperature difference of less than 5°F between the guard heater and the specimen. A steady-state condition was determined by periodically recording the temperatures of the metal specimens and the main heater. Steady-state conditions were usually achieved in six to eight hours. Generally the experimental runs, with and without interstitial materials, were conducted in the order of increasing load pressure.

The thermal contact conductance values listed in the Appendix A were obtained from the ratio of the interface heat flux to the junction temperature difference. The heat flux was calculated by the product of the thermal conductivity of the metal test specimen and the temperature gradient. In all tests one of the specimens was at a

more extreme temperature (+ 300°F or - 300°F), while the other was much nearer the ambient conditions of 70°F to 90°F. Since the temperature measurement error should be less and the assumption of one-dimensional heat flow better for the ambient temperature specimen, the heat flux calculated for this specimen was used in calculations of the thermal contact conductance. The temperature versus position plot for the metal test specimen was usually linear and the slope easily discernable. However, there exists some uncertainty in the selection of the "best" temperature gradient. This is especially true for the aluminum test specimens and interstitial materials with contact conductance values of less than 5 Btu per hr. ft^2°F. For this reason, a maximum and a minimum slope of the temperature gradient were estimated. This range of temperature gradient usually gave a difference between the high and low values of contact conductance of from 2 to 3 Btu per hr. ft^2°F for h values less than 10 Btu per hr.ft^2°F. The difficulty of ascertaining the "best" slope was increased with decreasing contact conductance. For example, with the aluminum test specimens and an interstitial material such as the felt* or laminate with a value of h less than 2 Btu per hr.ft^2°F, a zero temperature gradient can be obtained by allowing a deviation of 1/2°F in the temperature readings. Thus, to provide a better estimate of the thermal contact conductance for these extreme cases (low values of h), the heat flux was also calculated by determining the energy losses from the heated specimen. This method is discussed later in this chapter.

* Interstitial Materials are listed in Table 2.

Since the thermal conductivity of the metal specimens (which act as heat meters) is essential to the calculation of the thermal contact conductance, an apparatus to experimentally verify the use of the published values of thermal conductivity was constructed. The apparatus consisted of a central heater sandwiched between two 1 5/8" diameter x 4" cylinders of the test material. Each end of this test column was attached to a liquid cooled plate and heater combination. A selected temperature gradient could be maintained by adjusting heater power inputs. Temperatures were obtained from thermocouples inserted into the test material at one-half inch intervals. The experimental results verified the use of published values of the thermal conductivity. A discussion of these results is given in Reference (24). The thermal conductivity values which were selected are from References (10,27) and are graphically illustrated in Figure 9.

Metal Test Specimen and Interstitial Material Preparation

Since the surface finish of the metal test specimens (heat meters) could influence the thermal contact resistance, the contact surfaces were carefully finished in an identical manner for all test specimens. Each specimen, after it was machined, was placed in a brass jig which held the specimen in a vertical position and the contact surfaces lapped on a Lapmaster 12. After the lapping process the specimen was polished to remove any oxide layers. The surface was then checked for flatness deviation by interference refraction of a helium light source on an optical flat of quartz glass. Traces of the surface profiles were also obtained with a Bendix Micrometrical

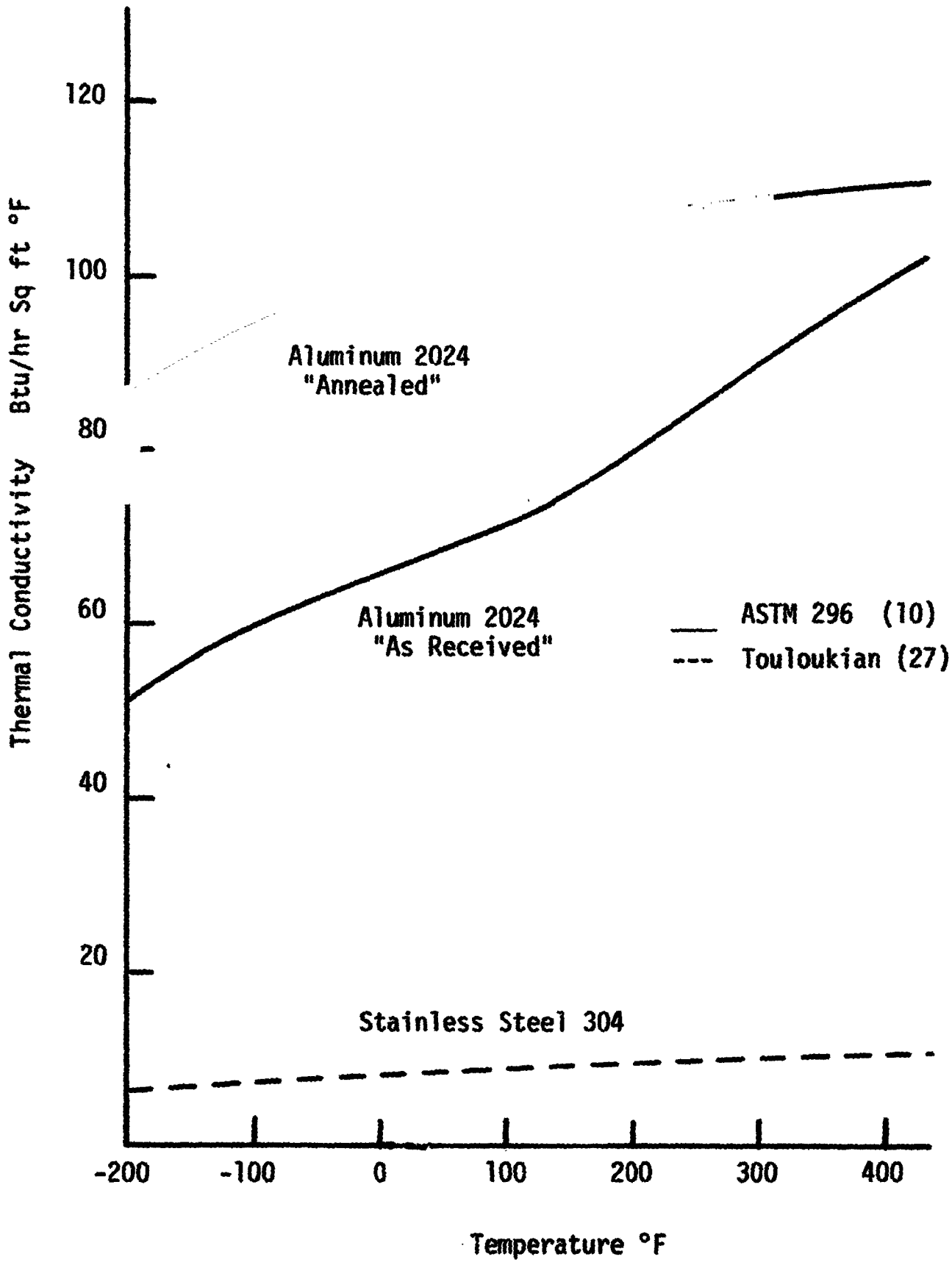

FIGURE 9. The Variation of Thermal Conductivity with Temperature for Stainless Steel 304 and Aluminum 2024.

Proficorder and profilometer. The resulting surface for each of the specimens was found to have a flatness of 20-25 μ in. and a roughness of 3-5 μ in.

Abbott (1) had previously considered several different techniques for constructing and installing the thermocouples in the metal specimens. The method which he suggested was followed for the test specimens used in this investigation. The thermocouples were constructed by twisting approximately one-fourth inch of the copper and constantan wires together. Then to improve the mechanical strength the junction was silver soldered. After which the excess wire was trimmed to the point where the wires first made contact. The completed thermocouples were installed in the specimen by carefully packing the cavity around the thermocouple with aluminum powder. An x-ray of the first two sets of aluminum specimens was made to ascertain any drill run-out, discontinuity of the thermocouple, or improper packing of the thermocouple. Since the specimens were found to be dimensionally correct and the thermocouples well-packed, the x-ray procedure was deemed unnecessary for later specimens. As a final check the continuity of the thermocouples was checked before and after packing by measuring their electrical resistance. During the thermal tests the surface and centerline thermocouples generally agreed within 0.5°F. Only in the extreme temperature cases of + 300°F and - 300°F did they deviate from one another as much as 2°F. To reduce heat transfer from the thermocouple junction the thermocouple leads were wrapped tightly around the specimen.

Since the interstitial materials were usually in bulk form,

The preparation of the test specimens involved the cutting of the materials into one inch diameter disks and the cleaning of the disks to insure that there was no contamination which could effect the test results. Initial thickness of the test specimens were taken for the purpose of determining any permanent deformation which was due to the applied pressures and temperatures during each test series.

Calculation Techniques

Thermal contact conductance is defined

$$h = q/\Delta T$$

The axial temperatures in the metal specimens were plotted versus distance from the interface, and extrapolated to the interface by a least-square fit to the measured temperatures. Hence ΔT was simply the difference between the junction temperatures found for the high and the low temperature specimens. Since the thermal conductivity of the metal test specimens was known (Figure 9), the heat flux, q, was calculated as the product of the temperature gradient in the metal specimen nearest room temperature and the thermal conductivity. This method of calculation proved to be very satisfactory for the bare junction runs and for materials having thermal conductance values greater than 10 Btu/hr ft^2°F. However, as indicated earlier in this chapter, there is a degree of difficulty in ascertaining the "best" slope. This uncertainty becomes extremely important in the calculation of q when the temperature gradient is on the order of 1°F per inch. For these low heat flux runs the heat flux was calculated by

an energy balance on the heated specimens (11).

The procedure for calibrating the apparatus for the energy loss from the heated specimen was essentially the same whether liquid nitrogen or chilled water was the coolant. The main difference being the temperatures of the specimens. With water the heated specimen was operated at temperatures up to 300°F but with liquid nitrogen the heater surface was maintained at approximately 100°F. Power input to the heater was measured at several different heater surface temperatures with the metal test specimens contact surfaces separated slightly in the vacuum environment. Coolant flow was maintained to obtain specimen and radiation shield temperatures close to those encountered during tests of interstitial materials. The emissivities of the aluminum and the stainless steel specimen surfaces were estimated as 0.2. Since the temperatures of the specimens and shields were measured, the heat transferred by radiation from the instrumented section of the heated specimen to the radiation shield, and from one specimen to the other across the gap at the contact could be estimated. Subtracting these losses, an estimated loss for the thermocouple leads, and a heater I^2R loss from the power input gave the energy transferred from the heater region by radiation. For the calibration runs the guard heater was monitored very closely to maintain a small temperature difference across the axial insulator separating the metal specimen from the guard heater (less than 3°F). Division of the heat loss, Q_ℓ, from the heater by the temperature to the fourth power difference between heater surface and shield yielded a heat loss coefficient for the heater region. Thus the

junction heat transfer for the low heat flux runs could be estimated very closely by subtracting the calculated energy losses from the heater power input.

$$Q_j = Q_{input} - I^2r - Q_\ell - [\text{specimen surface radiation loss and thermocouple loss}]$$

where Q_j is the heat transfer at the junction and Q_ℓ is the radiation loss from the heater surface which is calculated with the heat loss coefficient and the heater and shield temperatures.

For the higher junction temperature runs (aluminum specimens) with water as the coolant the junction temperature difference was approximately 200°F, so for an error in Q_j of one Btu/hr an error of 0.9 Btu/hr ft^2°F in h would result. However, comparison with the h values determined with the thermal conductivity and temperature gradient for the higher heat flux cases such as asbestos board at 100 and 300 psi and carbon paper at 300 psi indicates that the error in h is within 0.2 Btu/hr ft^2°F. Thus the uncertainty in calculating Q_j by the heat loss calibration can be estimated as 0.2 to 0.3 Btu/hr. As a result of the difficulty with measuring the temperature gradient for a small junction heat flux, stainless steel specimens were constructed to replace the aluminum. With an assumed maximum uncertainty in the temperature slope of 0.5°F/inch the approximate uncertainties in the calculated heat transfer for the different specimens (heat meters) are:

annealed aluminum	3 Btu/hr
as received aluminum	2 Btu/hr
stainless steel	0.3 Btu/hr

For comparison, the high temperature runs with the heated specimen at 300°F generally gave a ΔT of approximately 200°F for the better insulating materials. With this ΔT and the uncertainty in the calculated heat transfer the approximate uncertainty in h would be:

annealed aluminum	3 Btu/hr ft^2°F
as received aluminum	2 Btu/hr ft^2°F
stainless steel	0.3 Btu/hr ft^2°F

These values would be reduced slightly for the cold runs since the ΔT was increased in those runs to as much as 400°F. Therefore, the energy balance method is preferred for use with the aluminum specimens when the temperature gradient is less than 1 to 1 1/2 °F/inch, which corresponds to values of h between 5 and 7 Btu/hr ft^2°F for the high temperature runs. On the other hand with stainless steel specimens the uncertainty in h for either method of calculating Q_j seems to be approximately the same, 0.3 Btu/hr ft^2°F. Although a heat balance calibration was performed with the stainless steel specimens the values of h calculated by k and the temperature gradient are preferred. The energy balance method will become less accurate with increased junction heat transfer because the heater thermocouple no longer gives a good representative value for the entire surface. Also during opening and closing the vacuum system to install new test samples the attachment of the thermocouples to the shields and the location of the shields can be inadvertently changed between runs. Thus the heat loss method was used only to check the order of magnitude of h and the operation of the test apparatus for the stainless steel runs.

Compression Tests

Since the initial thicknesses of the different interstitial materials are not the same and because the thickness, ℓ, varies with the load pressure, the comparison of the junction thermal resistance, $R = 1/hA$, for the different materials should account for the material thickness. A better comparison would be the thermal resistance per unit thickness R/ℓ. The inverse of this ratio, $\ell/R = h\ A\ \ell$, has the advantage of having a desired ultimate limit of zero rather than infinity. To obtain the necessary thickness information, compression tests were run on interstitial material samples that were similar to those used for the thermal tests. An initial test run to 1000 pounds was made without an interstitial material to measure any deflection in the compression apparatus. The apparatus itself consisted of two one-inch diameter aluminum rods with an attached extensometer. Since no deflection of the apparatus was encountered, one inch diameter test samples were measured for initial thickness with a micrometer and placed into position between the ends of the aluminum cylinders. A continuously increasing load was then applied up to 300 lbs with dial indicator readings taken at designated increments. The effective compressive strain ($\ell_o - \ell / \ell_o$) of the test materials are illustrated as a function of pressure in Figure 14. More details concerning the procedure followed for the compression tests are available in Reference (24).

To ascertain whether or not the compressive strain is influenced by the initial thickness, compression data were obtained for multi-layer samples of carbon paper and mica. For carbon paper one, three

and six layers were consecutively tested. The resulting compressive strain curves agreed within four percent of each other. However, this was not the case for mica in which one, three, and five layers were tested. It was observed that the compression strain values for three and five layers are less than the single layer by the approximate fractional relation of one over the number of layers. Fry (15) stated that his tests indicated that the thermal resistance of mica was due mainly to a surface contact resistance rather than the bulk material resistance. The compression curves could be explained as a surface effect which would agree with Fry's observation. In contrast with mica, the compressive strain for carbon paper which is a very pliable and loose material is independent of the initial thickness. Therefore, the thermal resistance of the carbon paper will be primarily a result of the effective thermal conductivity and not contact resistance.

CHAPTER IV

EXPERIMENTAL RESULTS

Good insulating materials are usually not compact. In fact, in a vacuum environment, the very small effective thermal conductivity of most materials is due in part to tne voids in the material. However, the application of any compressive mechanical load can cause an irreparable reduction in the insulating capability for such materials. Thus to insulate metal-to-metal contacts which are pressed together, for example in a bolted flange configuration, materials that can withstand compressive loads are necessary. Since the heat transfer at the insulated junction is a function of the thermal conductivity of the interstitial material and the contact area, the materials can be in the form of sheets or disks, powders, screens, or perforated disks. The supplier and the available manufacturers data for the interstitial materials that were tested are listed in Table 2. All of the thermal test results for these materials are tabulated in Appendix A. In this particular table the run numbers such as 4-CA-25 have the following significance:

1. The first digit represents the metal test specimen set for that run. Table A-1 in Appendix A lists the type of metal and the surface roughness and flatness deviations for the test specimens.

TABLE 2

MANUFACTURER'S PROPER γ DATA

MATERIAL	RUN SYMBOL	SUPPLIER	K Btu/hr.ft°F	ρ lb_m/ft^3	VACUUM WEIGHT / AIR WEIGHT
Asbestos Board	AB	Johns-Manville	~0.04 - 100°F ~0.06 - 500°F	136	---
Asbestos Tape (No. 2074)	AT	Atlas Asbestos Company	~0.12 - 300°F	~55	0.985
Carbon Paper F-907	CA	Fiberite Corp.	0.2 - 300°F	~9	0.993
Ceramic Paper 970-J	CE	Carborundum Company	0.03 - 400°F 0.10 -1600°F	~12	0.999
WRP-X-AQ Felt	FE	Refractory Products Co.	0.04 - 500°F 0.12 -2000°F	18	0.995
Laminate T-30LR	LA	Carborundum Company	0.37 - 250°F 0.13 -2000°F	~50	0.989
Magnesia 25	MA	Degussa Inc.	15.7 - 112°F	~196	---
Mica (Bonded)	MI	Regan Engineering	.21- 100°F 1.24 -1000°F	13	0.999
Pluton B-1 Cloth	PL	3 M Company	0.02 - 80°F 0.03 - 180°F	87	---
Pyroid	PY	Pyrogenics Incorporated	1.00 - 70°F 0.30 -5000°F	162	---
Silica Paper F-904	SI	Fiberite Corp.	~ 0.10 - 300°F	~10	0.992
S.S. Screen 10/in	SS 10	--	~9.30 - 212°F	~500	---

TABLE 2 (Cont'd)

MATERIAL	RUN SYMBOL	SUPPLIER	K Btu/hr.ft°F	ρ lb_m/ft^3	VACUUM WEIGHT / AIR WEIGHT
S.S. Screen 100/in	SS 100	---	~9.30 - 212°F	~500	---
Teflon Sheet	TE	DuPont Co.	1.35 - 100°F	~10	---
Titanium Screen 20/in	TI 10	Newark Wire Cloth Company	~11.6 - 200°F	~276	
Tungsten Screen 20/in	W20	Newark Wire Cloth Company	~96 - 32°F ~70 - 932°F	~1210	---
Zirconia 23	ZI	Degussa Inc.	~1.08 - 212°F	~355	---

2. The letter code represents the type of interstitial material. These are defined in Table 2. In the example used, CA means carbon paper.
3. The final digits correspond to the test run in chronological order for a particular set of metal test specimens, i.e. in the example chosen this is the twenty-fifth run with specimen set 4.

In addition to the various interstitial material tests, runs without interstitial materials were also conducted with each test specimen set. The purposes for these bare junction tests were to provide a comparison for the insulating materials and to check whether or not the test specimen surface conditions had changed. Test results for the bare junction runs are also tabulated in Appendix A (Table A-2).

Bare Junction Tests

The test results through run 4-BJ-31 with Aluminum 2024 specimens have previously been reported in Reference(24). However, all of the results have been repeated in Table A-2 of Appendix A for completeness. The initial specimens (set 1) were machined from "as received" aluminum stock. After several test runs at the higher temperatures, an obvious change in the material properties of the heated specimen was observed. For example, it was noted that the ratio of the temperature gradient in the heated specimen to that in the cooled specimen had increased from 1.28 to 1.4. This

new ratio of 1.4 corresponded to a thermal conductivity ratio of annealed aluminum in the heated specimen to as received aluminum in the cooled specimen. This property variation which must be attributed to a slow annealing of the heated specimen while subjected to a compressive load caused a definite change in the bare junction h values. These values starting from run 1-BJ-16 are shown by the flagged symbols in Figure 10. Thus in all of the comparative runs with specimen set 1, from run 1-SI-13 on, the heated specimen was considered as annealed and the cooled specimen as "as received". Since the heat transferred was calculated by the temperature gradient in the cooled specimen, the h values for interstitial materials found with set 1 were not effected. This was confirmed by later repeat runs with other metal test specimen sets. To assure that the metal properties would not change in future tests, beginning with set 2 all aluminum specimens were annealed by heating in an oven to 600°F for twenty-four hours prior to finishing the contact surface.

Many bare junction tests were interspersed between the interstitial material runs to check for changes in the surface conditions. In some cases large variations in the h values from those of previous runs were observed. These were found to be the result of some surface change such as oxidation, contamination by the previous interstitial material, or a scratch or imperfection. Only initial test runs with each specimen set (i.e. before interstitial material runs or test runs after cleaning the contact surfaces)are plotted in

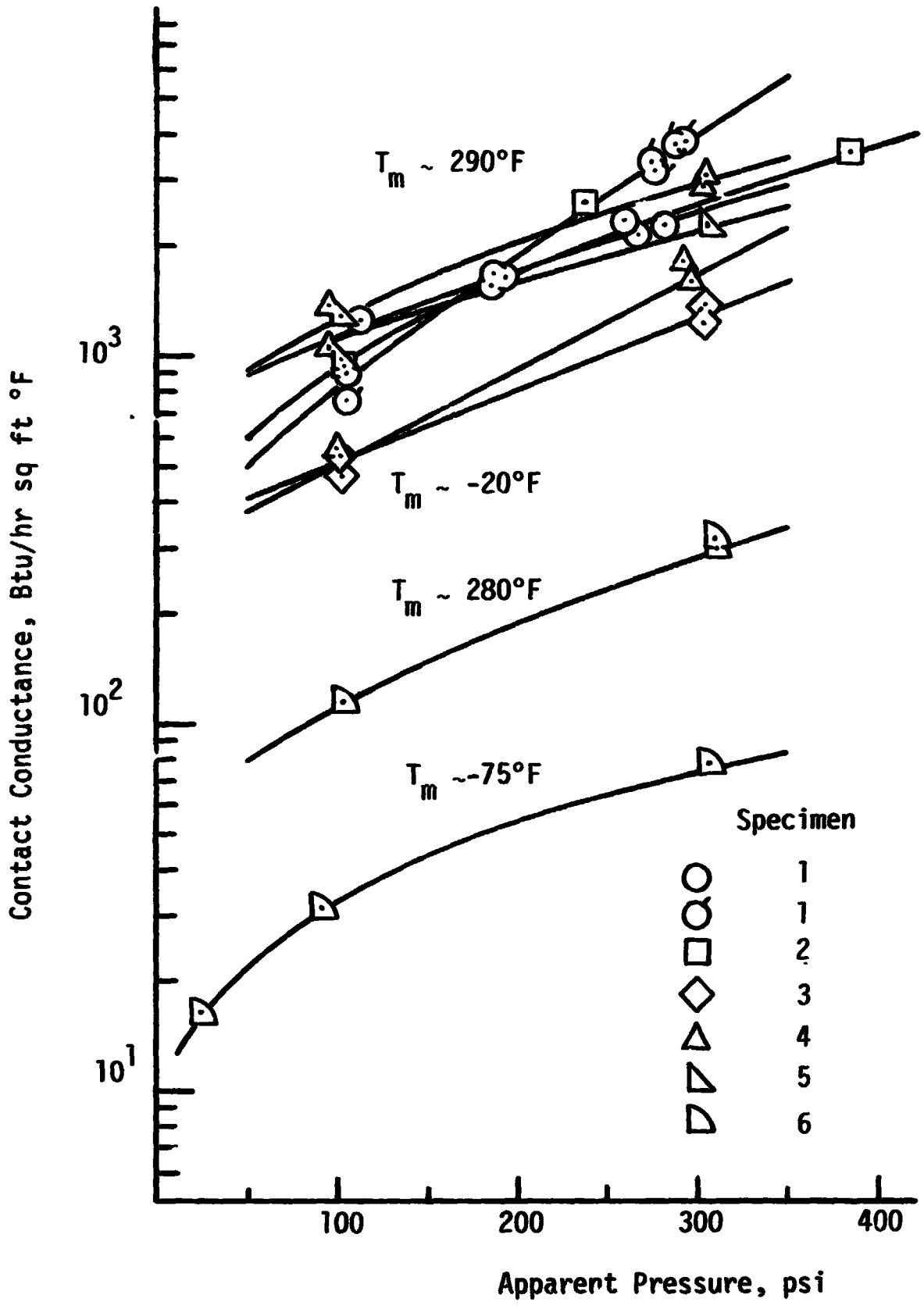

FIGURE 10. Thermal Contact Conductance of Bare Junctions

Figure 10 to establish a bare junction curve for comparison with interstitial material values. The aluminum was extremely prone to contamination and oxidation. To limit the degree of oxidation the test specimens were allowed to cool in the vacuum chamber after a test. Then nitrogen gas was released into the vacuum chamber to aid in the final cooling before opening the bell jar. As an example of the effect of contamination, run 4-BJ-20 decreased to 55 percent of the value of the previous run 4-BJ-17. It was observed that materials such as the felt, laminate, and ceramic paper leave a slight residue on the contact surfaces after a test. After cleaning the contact surface the h value for the subsequent run, 4-BJ-30, increased by 11 percent over the previous run. Similar situations were observed between runs 4-BJ-40 and 41, and runs 4-BJ-1 and 9. Small imperfections in the form of oblong dents were left in the aluminum metal specimen surfaces after the screen tests. The subsequent bare junction run (1-BJ-63) showed a large decrease in h as would be expected. Also previous investigators, such as Fried (13) and Clausing and Chao (7), have found that the deviation in their smooth surface h values is greatly increased over that for rough surfaces.

Interstitial Materials

A summary of all of the test results for the seventeen interstitial materials listed in Table A-3 is given in Appendix A. A discussion of the uncertainty in h values is presented in Appendix B.

For the purpose of comparing the insulating performance of the materials a first series of runs from 100 psi to 300 psi load pressure was conducted with each of the different materials and aluminum specimen sets 1 and 2 (Runs I-SI-13 through 2-SS10-18). These comparison runs were all at an average junction temperature of approximately 200°F. Cold runs 3-AB-6 through 3-SS10-24 with liquid nitrogen as the coolant were next run with specimen set 3 and some of the better insulators to obtain a comparison between a 200°F and a -100°F mean junction temperature. As a result of the comparison tests, the seven materials which had the lowest h values were rerun with specimen sets 3 and 4 to test the repeatability of the experimental results. These repeat runs were conducted for both the high and the low junction temperatures and the results agreed very closely with the previous values of h. Special runs such as increasing and decreasing load, rougher surface and multilayers were conducted with specimen set 5. On page 27, the difficulty of measuring temperature gradients was explained. To alleviate this problem stainless steel 304 specimens (set 6) were constructed. Since the ratio of the thermal conductivity of the aluminum to the stainless steel is approximately 10, the temperature gradients were increased to easily determined magnitudes.

A second series (MIB)* of runs were made on mica to check the repeatability of the mica data. The resulting h values were approximately 50 percent of those obtained in the first runs (MI)*. The

*Re... ...in Table A-3

mica used was supplied by a local heater manufacturer and was considered an economy grade which refers to the presence of relatively large areas of discoloration. These discolorations indicate impurities such as silicon and iron oxides. To see if this had any effect another specimen (MIG)* from the same batch of mica sheets with a black-gray discoloration, instead of the reddish-brown color which was used in the second series, was tested at a load of 100 psi. The resulting h value was approximately 83 percent of the initial value at the same pressure. A subsequent bare junction run indicated that the surfaces were oxidized. After clearning the surfaces, another specimen containing the same discoloration as the previous one was run at 100 psi. An h value of approximately 96 percent of the initial was obtained. Although the low h values obtained for the second set of runs could be attributed somewhat to oxidation of the aluminum specimen surfaces, it seemed more likely that impurities in the mica, and perhaps possible misalignment of the specimens were more probable reasons. Therefore, to avoid the problem of variations in the test samples a better grade of mica (clear grade) was ordered and then tested to demonstrate the repeatability of mica data. This series of runs (MIC)* were conducted with stainless steel 304 metal specimens and yielded h values within ten percent of the second set of runs. Recent testing with the clear grade of mica found that the experimental data to compare. The results of these additional tests will be presented in a future report.

---

*Refers to notation in Table A-3

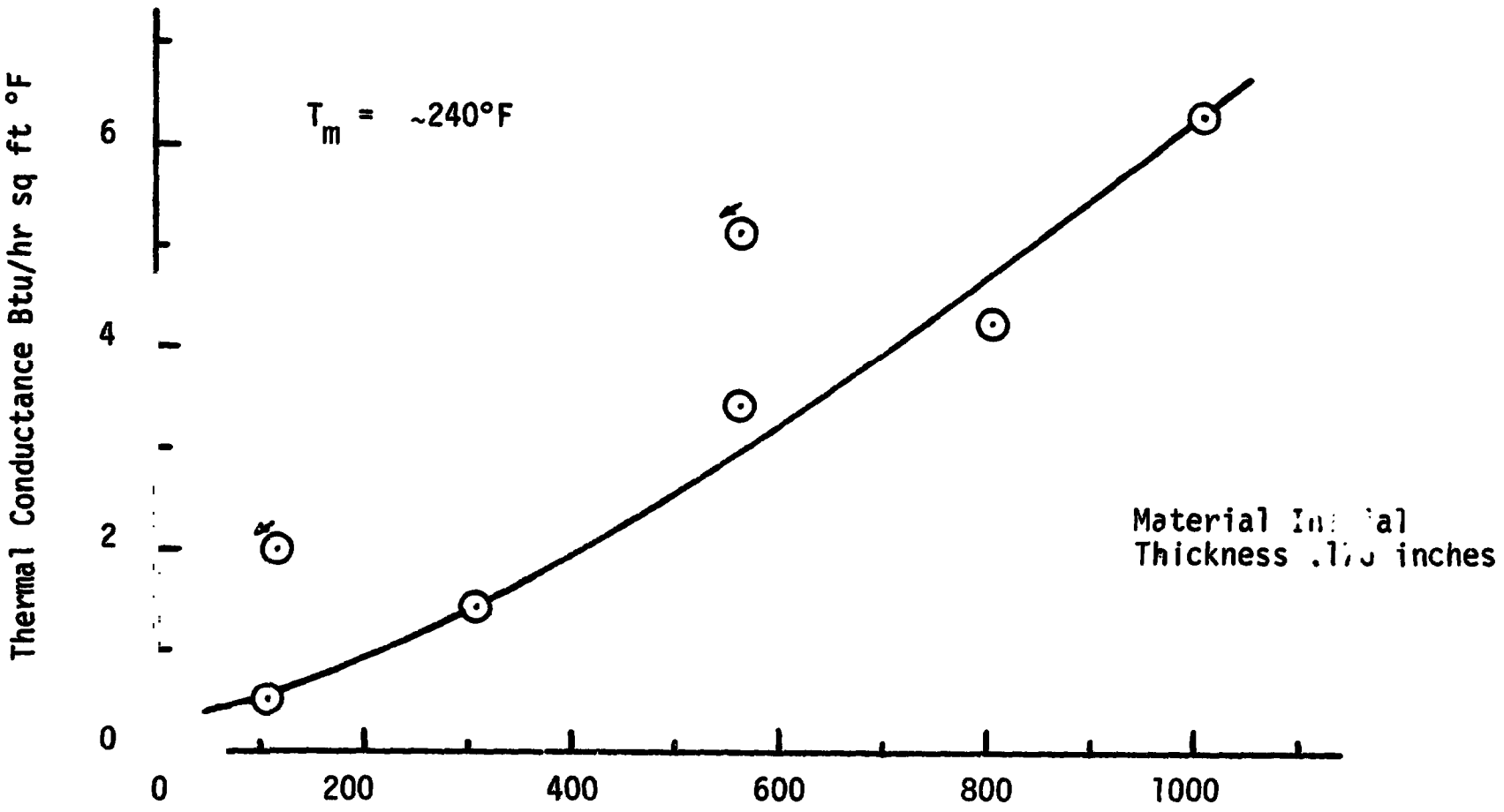

FIGURE 11. Thermal Contact Conductance of WRP-X-AQ Felt

To demonstrate the effects of initially compressing the sheet materials a series of increasing load pressure runs to 1000 psi and two return runs at reduced loads of 550 psi and 100 psi were conducted with a single layer of (0.176 inches thick) WRP-X-AQ felt (Figure 11). These runs were made with annealed aluminum specimens with average test specimen temperatures of approximately 300°F and 70°F (Runs 4-FE-44 through 4-FE-50). The increases in thermal contact conductance for 500 and 100 psi were 50.3 and 233 percent, respectively.

For the purpose of determining the magnitude of the effect of metal specimen contact-surface roughness, the low temperature specimen for set 5 (i.e., attached to the sink) was refinished with a lathe cut. This artificially roughened the surface to approximately 200 μ - inch roughness with a circular pattern but with no appreciable change in the flatness. Three bare junction runs were made with this new surface at 100 and 300 psi and a repeat run at 100 psi (Runs 5-BJ-1, 5-BJ-2, 5-BJ-6). The resulting h values were found to be 20 to 21 percent lower and 7 percent higher than the respective values established by the runs 4-BJ-19, 20, and 40. Clausing and Chao (7) found that the microscopic constriction resistances was negligible by comparison with the macroscopic resistance. Therefore, it appears that the roughened surface did not appreciably effect the macroscopic resistance. A change in surface flatness however may have a much larger effect. Subsequent runs at 300 psi with carbon paper (5-CA-4) and asbestos board

(5-AB-3) did not deviate from the values obtained with the smoother surfaces. Since these materials demonstrate a thermal resistance due to a bulk material resistance, this would be expected. The run with mica (5-MIC-5) gave a lower h value than with the smooth specimen surface (6-MIC-20) by 9 percent. Again, this is expected if a junction co..tact surface resistance is important for mica.

Since the h values measured with stainless steel specimens (set 6) are in agreement with the previous results with aluminum specimens it is concluded that the metal surface hardness does not have an appreciable effect on the layer or sheet materials. However, recent tests with stainless steel screens and stainless steel specimens demonstrate the expected reduction in h with increased hardness. The details of the tests with screens will be discussed in a future report.

Multi-layer tests were conducted on mica (5 layers which have an overall initial thickness of 0.0172 inches) and carbon paper (6 layers which have an overall thickness of 0.330 inches) at pressures of 100 psi and 300 psi. The test results for these runs are compared in Table 3. Although the multilayer configurations for both materials decrease the overall junction thermal conductance, h, the different behavior between these two types of material is illustrated. The ratio of the compressed thickness of a single to a five layer stack of carbon paper disks is compared with the ratio of the resulting junction h values. Hence, the product, $h\ell$, is a constant (within the experimental uncertainty) for materials like

carbon paper, so the junction thermal conductance is a function of the thermal resistance of the interstitial material and not the surface contact. In contrast to this the same comparisons for mica show that a surface contact resistance, which varies with load pressure, is present. Hence the junction thermal conductance is not decreased by a ratio of thicknesses but is a reduced factor of the thickness ratio.

TABLE 3

TABULATED RESULTS OF MULTILAYER TEST

RUN	P_a Psi	T_m °F	h Btu/hr ft^2°F	h Ratio	ℓ in	ℓ Ratio
6-CA6-9	112	192	0.89	6.57	.14260	6.00
6-CA-13	108	204	5.85		.02390	
6-CA6-10	313	193	1.80	6.22	.11150	6.23
6-CA-14	315	211	11.2		.01790	
6-MIC5-15	107	216	9.09	3.55	.01623	6.62
6-M. 9	106	253	32.3		.00245	
6-MIC5-16	312	227	16.8	3.90	.01596	6.91
6-MIC-20	309	268	65.5		.00231	

Since the heat transferred at a junction between metal surfaces is significantly effected by small variations in the contact area, the insulating effect of an interstitial material that reduces the heat transfer area is obvious. Perforated sheets, artificially roughened or corrogated surfaces, and wire screens represent such geometric insulation materials. Wire screens have the advantage of limiting the contact area with the plane metal surface to the regions where the wire weave of the screen overlaps. Also, the inner contacts of the wire, because of the woven structure, offer additional resistance to heat transfer.

Three different screen wire materials were tested, stainless steel, tungsten, and titanium. The test results are tabulated in Table A-3. To acquire a better understanding of the geometric resistance (screens) case, values of load per contact (L_c) and resistance per contact (R_c) were calculated (Table 4). Contact points are assumed to occur where the screen wire weave overlaps. In one square inch of surface area the number of such points is approximately equal to the mesh size squared. As the mesh size is increased, R_c is also increased while L_c is decreased as shown by 10 and 100 mesh stainless steel screens. Thus on a per contact basis, the thermal resistance of the 100 mesh screen is greater than the 10 mesh screen because of the smaller wire diameter. However, the contact point resistances are in parallel and yield a lower overall resistance for the 100 mesh screen as result of the larger number of contacts. Since the load per contact is known an area per contact which would be a function of

L_c could be calculated. Because the load pressure per contact is large it can be assumed that the thermal resistance is due to a geometric and a material resistance in series. With this procedure, the value for R_c can be predicted for the screen wire. A study of a technique for predicting the thermal resistance for screens will be presented in a future report.

TABLE 4

TABULATED EXPERIMENTAL DATA
FOR SCREEN CASES

RUN NO.	WIRE DIA. in.	LOAD/CONTACT lb.	RESISTANCE/CONTACT Hr °F/Btu
2-SS10-16	0.025	1.32×10^{0}	8.32×10^{2}
2-SS10-17	0.025	1.92×10^{0}	7.39×10^{2}
2-SS10-18	0.025	2.79×10^{0}	6.02×10^{2}
3-SS10-23	0.025	1.04×10^{0}	1.95×10^{3}
3-SS10-24	0.025	2.99×10^{0}	1.13×10^{3}
1-SS100-57	0.004	0.96×10^{-2}	2.23×10^{4}
1-SS100-58	0.004	1.87×10^{-2}	1.60×10^{4}
1-SS100-59	0.004	2.77×10^{-2}	1.56×10^{4}
1-TI10-60	0.025	1.02×10^{0}	13.45×10^{2}
1-TI10-61	0.025	1.86×10^{0}	8.83×10^{2}
1-TI10-62	0.025	2.75×10^{0}	6.58×10^{2}
1-W-2064	.007	0.25×10^{-1}	4.88×10^{2}
1-W-2065	.007	0.47×10^{-1}	3.79×10^{2}
1-W-2066	.007	0.69×10^{-1}	3.10×10^{2}

A graphical comparison of the junction heat transfer for aluminum specimens with and without interstitial materials is given in Figure 12. The curves were plotted for the average of all runs with water as the coolant and the heated specimen at approximately 300°F. Since the 100 mesh SS screen is probably on the upper extreme of the desirable materials (on the basis of h), all of the better insulating materials such as laminate, mica, ceramic paper, etc., will be between the 100 mesh screen and the 6 layer carbon paper lines. The 6 layer carbon paper insulation reduces the junction heat transfer to less than one percent of the bare junction value.

Since the initial thicknesses of the interstitial materials varied, a direct comparison of the experimental values of the junction thermal contact conductance is not sufficient. If surface contact effects are neglected and a linear temperature gradient assumed for the interstitial material then,

$$Q_j = h A \Delta T = k_e A \frac{\Delta T}{\ell}$$

where ℓ is the thickness of the interstitial material and k_e is an effective thermal conductivity. Thus for this solid layer of insulating material

$$k_e = h\ell$$

A good thermal insulating material would therefore have a very low value for the product $h\ell$. This is compared as a function of pressure for all of the materials tested in Figure 13. However, the compression strain (Figure 14) curves used to calculate were obtained at room temperature, and some deviation in these curves could be

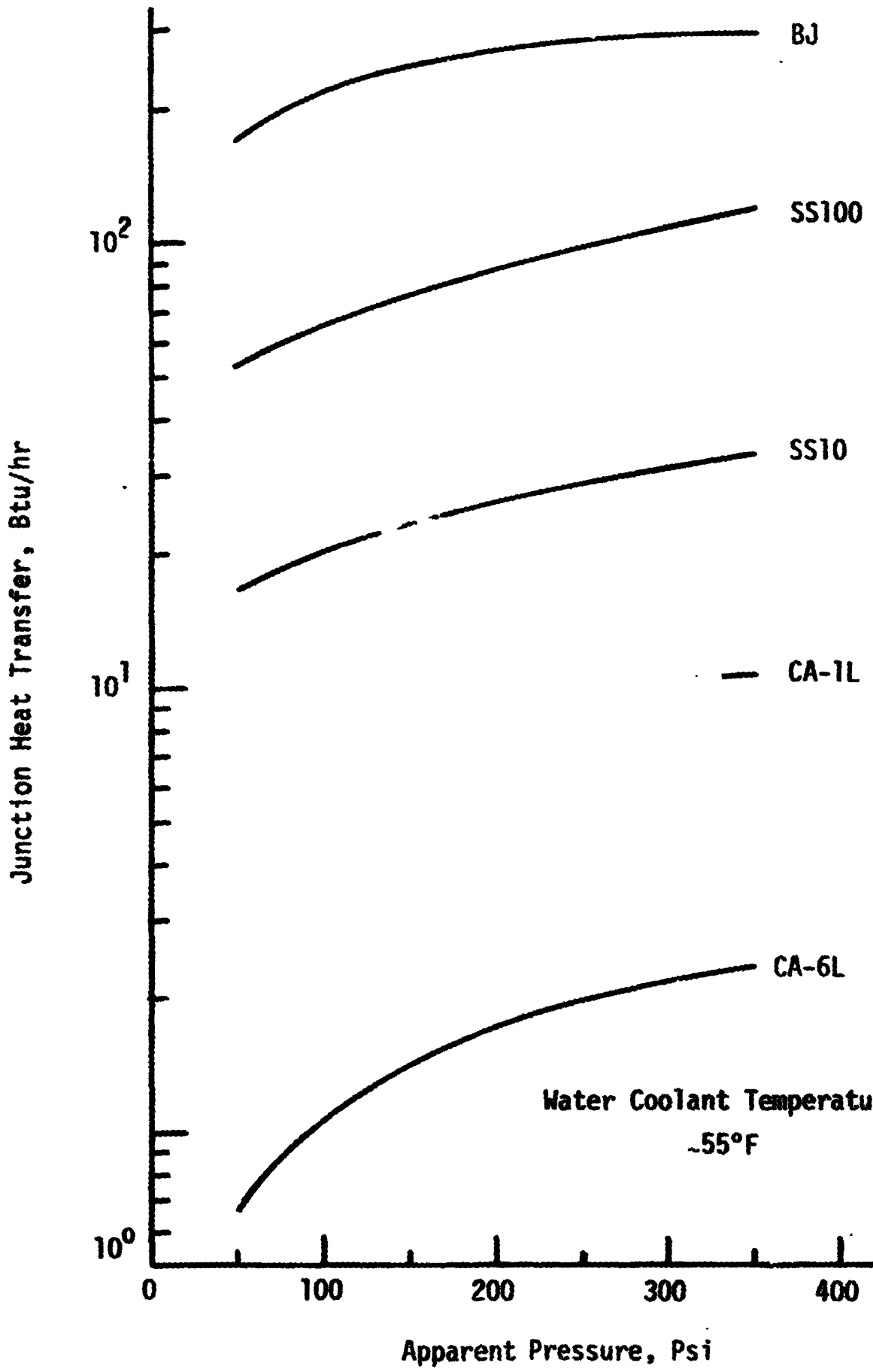

FIGURE 12 Comparison on Junction Heat Transfer With and Without Interstitial Materials.

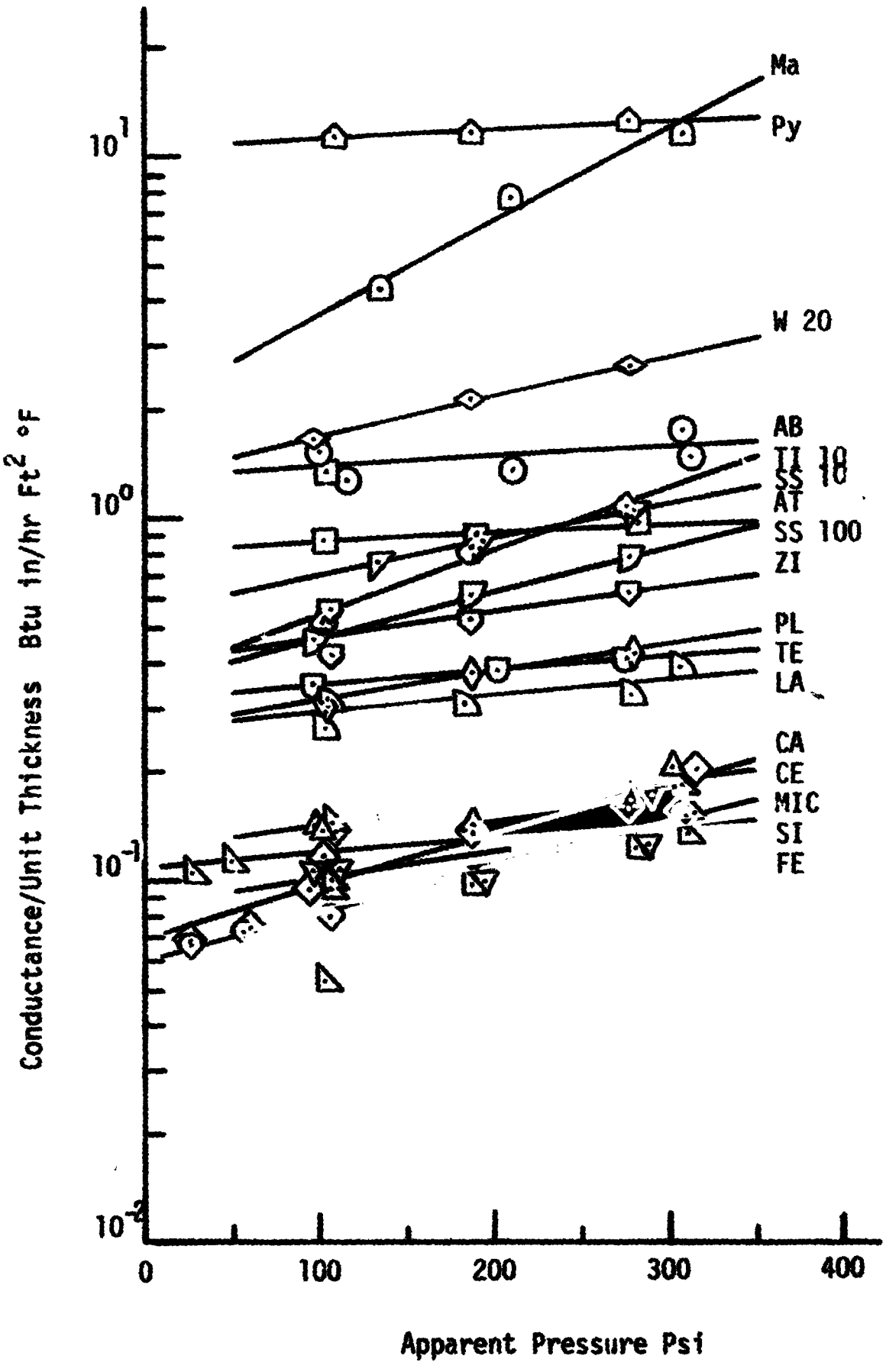

FIGURE 13. Thermal Conductance Curves per Unit Thickness Curve

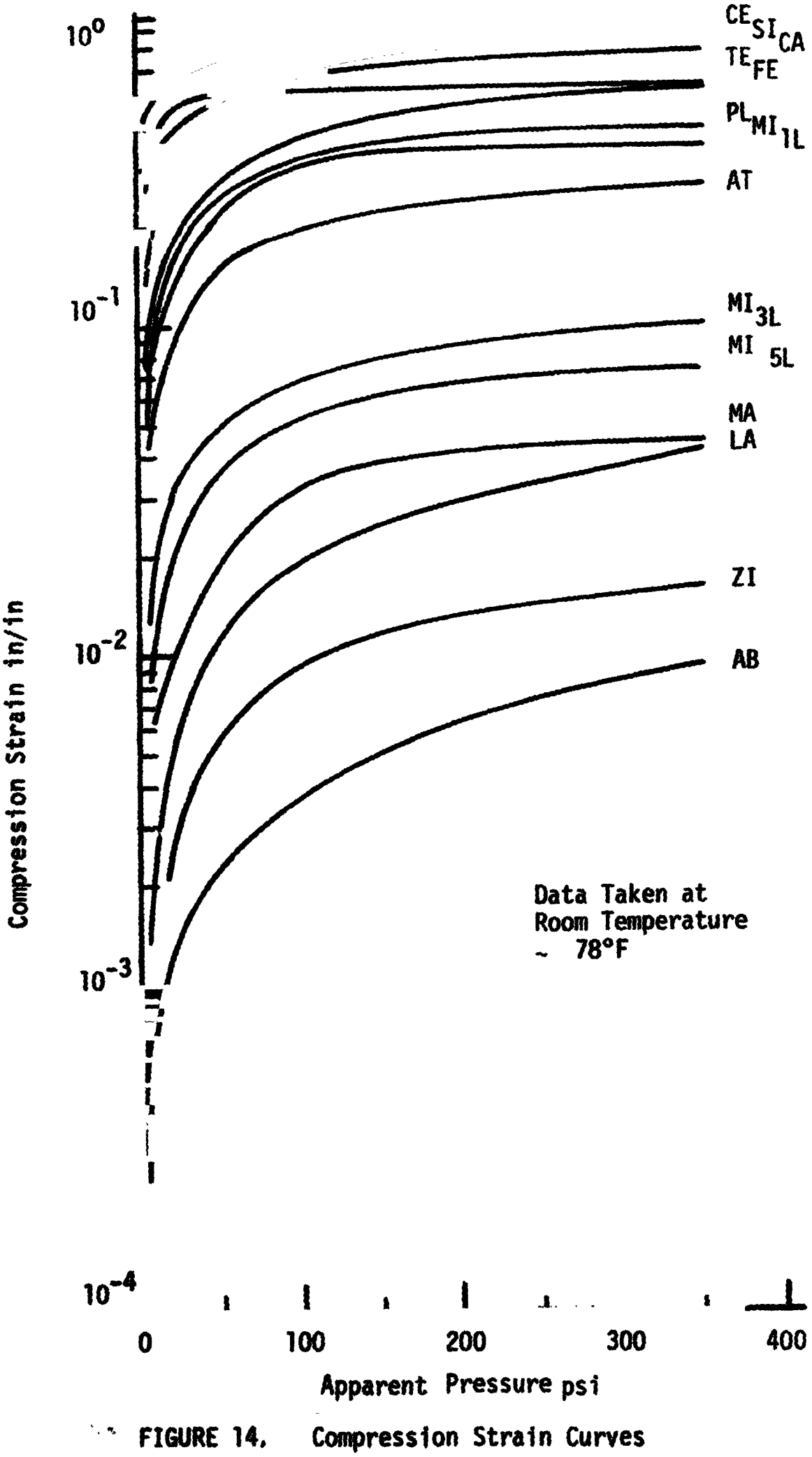

FIGURE 14. Compression Strain Curves

encountered at higher or lower temperatures depending upon the expansion or contraction of the material with temperature. Since the sides of the disk are free, it is assumed that any possible deviation in ℓ can be neglected for the purpose of comparing one material to another in Figure 13. On this basis, carbon paper, ceramic paper, mica, silica paper, and WRP-AQ felt appear to be the better materials.

Although the test values are not plotted, with liquid nitrogen coolant the mean junction temperature was reduced to approximately -150°F with the aluminum specimens. The effect was to reduce the values of h in all cases except mica. These reductions were generally from 10 to 40 percent of the values for the higher temperature runs. In some cases, notably the pluton B-1 cloth, the reduction was as much as 60 percent. It is surmised that reductions in h can be primarily attributed to a reduction in the thermal conductivity with temperature. However, mica seems to behave in an opposite manner with almost a 10 percent increase in h for a reduction in mean temperature from 260°F to -8°F (Table A-3 runs 6-MIC-17 through 6-MIC-26). Several factors are involved so it is difficult to give a quantitative explanation for mica. The sheets from which the test samples were cut varied in thickness. For the high temperature runs the initial thickness of the test sample as measured with a micrometer was 0.0034 inches whereas the test sample for the low temperature runs was 0.0028 inches. If the bulk thermal resistance of the material (i.e. ℓ/kA) is predominate the h values for

the high temperature runs could be increased by a ratio of thicknesses for comparison with the lower temperature runs. Thus the h for run 6-MIC-19 would be increased to 39.2 to be compared with h = 35.7 Btu/hr ft^2°F for run 6-MIC-25. The multilayer test results in Table 3 show that the h value of mica would not be increased by the factor of the ratio of thicknesses but only by 53.6 percent of the ratio of thicknesses. Therefore, with a 0.0028 inch sample the h calculated for run 6-MIC-19 would be estimated to increase to 36.0 Btu/hr ft^2°F. If, as the evidence seems to indicate, the junction thermal resistance is due in part to a surface contact resistance the thickness variation would not be as important. In fact at the same load pressure and junction temperature the junction thermal contact conductance h would change only a negligible amount (15). By comparison with other materials the contact resistance could reasonably be assumed to decrease with junction temperature. Hence the test results including the temperature comparison runs imply that the junction thermal resistance for mica is a function of both the material thermal resistance and a contact resistance.

The primary purpose of a low conductance interstitial material is to minimize the heat transfer between contacting surfaces for a given temperature difference. Simply, the ratio $Q_j/\Delta T$ should be a minimum. By definition it follows that hA which is equal to $k_e A$ should therefore be a minimum, i.e. or the inverse 1/hA which is equivalent to the thermal resistance should be a maximum. This is obtained by requiring that the effective thermal conductivity of the

material $k_e = h\ell$ be a minimum. In addition, for spacecraft especially, the required weight may be of importance. This implies that the effective density ρ_e, of the material should be a minimum. Combining these criteria, with each being considered equally, the product

$$k_e \rho_e = \frac{he}{A}$$

should be minimized. Since all test samples had the same cross-sectional area only hw is plotted in Figure 15. The vacuum weight was used in the calculation of hw. These were obtained with a Cahn Model RG Electrobalance. Small but representative samples of the materials were first weighed in air and then in a vacuum. The ratio of these two measurements is listed in Table 2 and it was assumed that the "in air" scale weight of the thermal test samples would be reduced by this factor in a vacuum.

In the case of screens the mass of the test samples was calculated from the total length of the wire, the wire diameter, and the wire densities. Values for the densities of stainless steel, tungsten and titanium were taken from the eighth edition of the Metals Handbook (21).

$$\rho_{SS} = \sim 500 \text{ lb/ft}^3$$

$$\rho_W = \sim 276 \text{ lb/ft}^3$$

$$\rho_{Ti} = \sim 1210 \text{ lb/ft}^3$$

Since 1/h is proportional to the thermal resistance, the product hw can be interpreted as the mass/thermal resistance. Thus the value of this parameter should be a minimum for the better materials. From Figure 15, the magnitude of hw for titanium screen is 13.2

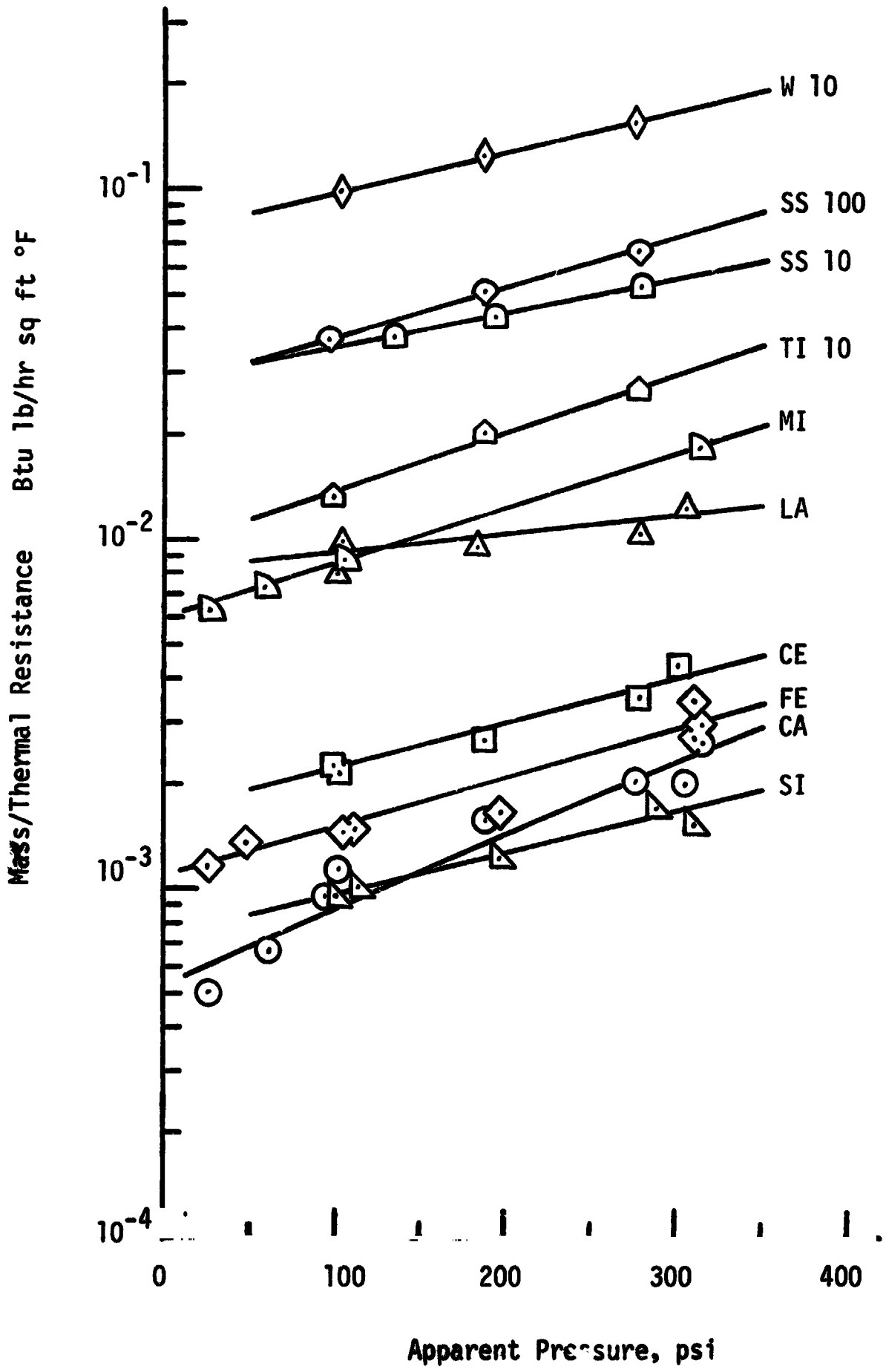

FIGURE 15. Mass Per Thermal Resistance Curves

x 10^{-3}, 20.1 x 10^{-3} and 27.0 x 10^{-3} Btu lb/hr ft^2°F at 99,186 and 278 psi, respectively, and would therefore provide largest junction thermal resistance per unit mass for the screen case. However, with weight and thermal conductance as the criterion for selection, the carbon paper, ceramic paper, WPR-X-AQ felt and the silica paper appear to be the more desirable materials.

Another criterion of possible structural interest might be the required thickness of the interstitial material, but in any installation where a compressive load is applied the mechanical strength of the material must be considered. In static cases, no vibration or oscillations in load and temperature, the compressive strain curves (Figure 14) give the degree of compression. On the other hand, with variable load and temperature (expansion-contraction) conditions the material should be subjected to a variable load test. Thus, ceramic paper, felt, and carbon paper, were subjected to a cyclic loading test to compare their strength under compressive loads. The ceramic paper when cylced between ten and 500 pounds six times, and felt when cycled between ten and 800 pounds four times were found to disintegrate. The minimum and maximum thicknesses at their respective loads for the first, second and final cycle are given in Table 5. Carbon paper did not evidence the same failure. Although Figures 13 and 15 indicate that silica paper is also a good insulator, it was not considered for the cyclic loading test since it was found to discolor (possible bonding deterioration) during the high temperature test. In summary, on the basis of

mechanical strength, thermal resistance per unit thickness and mass per thermal resistance, carbon paper is overall the better material of those that have been considered. However, in an application where compressive load strength is of primary importance a material such as a wire screen should be considered.

TABLE 5

TABULATED COMPRESSION DATA

MATERIAL	LOAD RANGE Lb.	NUMBER OF CYCLES		THICKNESS FOR MINIMUM AND MAXIMUM LOADS in.		
				1st Cycle	2nd Cycle	Final Cycle
CA	10-500	6	10 lb	0.0458	0.0244	0.0215
			500 lb	0.0132	0.0127	0.0121
CE	10-500	6	10 lb	0.0682	0.0336	0.0251
			500 lb	0.0194	0.0185	0.0160
FE	10-800	4	10 lb	0.1614	0.1008	0.0958
			800 lb	0.0930	0.0910	0.0889

CHAPTER V

SUMMARY

Experimental values of the thermal contact conductance, h, for the seventeen interstitial materials listed in Table 2 are tabulated in Table A-3 of Appendix A. The uncertainty associated with the h values is discussed in Appendix B. The thermal resistance of the interstitial materials can be a function of a bulk material thermal resistance, and a surface contact resistance. Multilayer thermal and compression tests with carbon paper demonstrated that for the papers and other pliable fiber sheet materials, the thermal resistance is primarily a bulk material resistance (ℓ/kA). In contrast the mica demonstrates the existence of both a material thermal resistance and a surface contact resistance. Compression tests of mica also show that the effective compressive strain is a function of load and initial thickness. Impurities in the economy grades of mica were found to significantly effect the thermal resistance. Repeatable data can be obtained with mica by using a clear grade to avoid variations in the test samples. Wire screens offer a substantial decrease in the junction heat transfer with the advantage of not failing under large compressive loads. As expected the thermal resistance of wire screens is a function of the thermal conductivity of the wire but more importantly the wire diameter and mesh size. An increase in the aluminum specimen surface roughness to 200 μ-inch demonstrated that the h values for the insulating

materials is not a significant function of roughness. However, large changes in surface flatness could have an effect. A change in surface hardness, aluminum to stainless steel specimens, did not effect the h values for the insulating materials tested. Recent tests with stainless steel screens and stainless steel specimens show a decided decrease in h over that for aluminum specimens. This is a result of a decrease in the contact area.

Selection criteria were proposed for the insulating materials. These were an effective thermal conductivity, $h\ell$; the density, and the mechanical strenyth under repeated loads. On these bases the carbon paper was found to be the better material. However, if mechanical strength is of primary importance, wire screens should be considered.

Further work with wire screens is contemplated to test the effects of surface hardness and temperature. Also a technique for predicting the junction thermal resistance with wire screens should be developed. Additional tests with mica should be undertaken to provide more definitive proof that its thermal resistance is a sum of a contact resistance and a material resistance. Finally, additional variable thickness tests should be conducted to determine the behavior of other materials besides mica and carbon paper.

BIBLIOGRAPHY

1. Abbott, Rudolph Edward. "Experimental Facilities for Investigating Thermal Contact Conductance in a Vacuum Environment," Unpublished Master's report, Arizona State University, Department of Mechanical Engineering, Tempe, Arizona, 1967.

2. Barzelay, Martin E. "Range of Interface Thermal Conductance for Aircraft Joints," NACA TN 3295, May, 1955.

3. Berman, R. "Some Experiments on Thermal Contact at Low Temperatures," Journal of Applied Physics, 27:318-323, April, 1956.

4. Blum, Harold A. "Heat Transfer Across Surfaces in Contact: Practical Effects of Transient Temperature and Pressure Environments," NASA CR 69696, October, 1965.

5. Burnot, A. W. and F. F. Buckland. "Thermal Contact Resistance of Laminated and Machined Joints," Transactions of the ASME, 71:253-257, April, 1949.

6. Cetinkale, T. N. and Margaret Fishenden. "Thermal Conductance of Metal Surfaces in Contact," General Discussions on Heat Transfer, Conference of the Institution of Mechanical Engineers and ASME. London: Institution of Mechanical Engineers, 1951.

7. Clausing, A.M. and B.T. Chao. "Thermal Contact Resistance in a Vacuum Environment," ASME Paper No. 64-HT-16, August, 1964.

8. Cunnington, G.R., Jr. "Thermal Conductance of Filled Aluminum and Magnesium Joints in a Vacuum Environment," ASME Paper No. 64-WA/HT-40, November, 1964.

9. Daily, R.M., and W.E. Kasparek. "Thermal Contact Conductance in a Vacuum," NASA TM X-53004, May, 1964.

10. Eldridge, E.A. and H.W. Deem (eds.). "Report on Physical Properties of Metals and Alloys from Cryogenic to Elevated Temperatures," ASTM Special Technical Publication No. 296, April, 1961.

11. Fletcher, Leroy S., Paul A. Smuda, and Donald A. Gyorog. "Thermal Contact Resistance of Selected Low Conductance Interstitial Materials," AIAA Paper No. 68-31, January, 1968.

12. Fried, Erwin. "Thermal Joint Conductance in a Vacuum," ASME Paper 63-AHGT-18, March, 1963.

13. _____. "Study of Interface Thermal Contact Conductance, Summary Report," General Electric Company Document No. 65SD4395, 1965.

14. _____, and Frederick A. Costello. "Interface Thermal Contact Resistance Problem in Space Vehicles," ARS Journal, 32:237-243, February, 1962.

15. Fry, E.M. "Measurements of Contact Coefficients of Thermal Conductance," AIAA Paper No. 65-662, September, 1966.

16. Hargadon, Joseph M., Jr. "Thermal Interface Conductance of Thermoelectric Generator Hardware," ASME Paper No. 66-WA/NE-2, November, 1966.

17. Holm, Ragnar. Electric Contacts: Theory and Application, Fourth Edition. New York: Springer-Verlag, 1967.

18. Hudack, Larry J. "An Engineering Analysis of Heat Transfer Through Metallic Surfaces in Contact." Unpublished Master's report, Arizona State University, Department of Mechanical Engineering, Tempe, Arizona, 1965.

19. Jansson, Richard M. "The Heat Transfer Properties of Structural Elements for Space Instruments," M.I.T. Instrumentation Lab Report E-1173, June, 1962.

20. Laming, L.C. "Thermal Conductance of Machined Metal Contacts," International Developments in Heat Transfer, Proceedings of the 1961-62 Heat Transfer Conference. New York: ASME, 1962. Pp 65-76

21. Lyman, Taylor (ed.). Metals Handbook (8th ed.), Vol. I. Metal Park, Ohio: American Society for Metal, 1964.

22. Mikesell, R.P. and R.B. Scott. "Heat Conduction through Insulating Supports in Very Low Temperature Equipment." Journal of Research of the National Bureau of Standards, 57: 371-379, December, 1956.

23. Minges, Merrill L. "Thermal Contact Resistance: Volume 1 -- A Review of the Literature," Air Force Materials Laboratory, AFML-TR-54-375, April, 1966.

24. Smuda, P.A., L.S. Fletcher, and D.A. Gyorog. "Heat Transfer Between Surfaces in Contact: The Effect of Low Conductance Interstitial Materials; Part I: Experimental Verification of NASA Test Apparatus," NASA CR 73122, June, 1967.

25. Substad, W.R. "Thermal Contact Resistance Between Thin Plates in Vacuum," ASME Paper No. 65-HT-16, August, 1965.

26. Thomas, T.R. and S.D. Probert. "Thermal Resistances of Some Multilayer Contacts Under Statis Loads," International Journal of Heat and Mass Transfer, 9:739-754, February, 1966.

27. Touloukian, Y.S. (ed.). Metallic Elements and Their Alloys, Vol. I. Lafayette, Indiana: Thermophysical Properties Research Center, Purdue University, 1966.

28. Weills, N.D. and E.A. Ryder. "Thermal Resistance Measurements of Joints Formed Between Stationary Metal Surfaces," Transactions of the ASME, 71:259-267, April, 1949.

APPENDIX A

EXPERIMENTAL DATA

TABLE A-1

METAL SPECIMEN DESIGNATION

SPECIMEN NO.	MATERIAL TYPE		SURFACE CONDITIONS	
	Hot Specimen	Cold Specimen	Hot Specimen	Cold Specimen
1	Aluminum 2024 AN	Aluminum 2024 UN	A	A
2	Aluminum 2024 AN	Aluminum 2024 AN	A	A
3	Aluminum 2024 AN	Aluminum 2024 AN	A	A
4	Aluminum 2024 AN	Aluminum 2024 AN	A	A
5	Aluminum 2024 AN	Aluminum 2024 AN	A	B
6	Stainless Steel 304	Stainless Steel 304	A	A

Notation

AN - Specimens annealed at 600°F for 24 hrs.

UN - Specimen unannealed

A - Roughness 3-5 µin Flatness 20-25 µin

B - Roughness 200-225 µin Flatness 25-50 µin

TABLE A-2

TABULATED EXPERIMENTAL RESULTS

BARE JUNCTION SERIES

Run	P_a	T_m	ΔT	h
	Psi	°F	°F	Btu/hr sq ft °F
		Aluminum 2024		
1-BJ-1	114	280	34.5	1270
1-BJ-2	268	289	22.3	2190
1-BJ-3	418	291	14.3	3550
1-BJ-4	567	293	10.0	5240
1-BJ-5	732	294	8.6	6190
1-BJ-6	881	295	7.5	7190
1-BJ-7	1038	296	6.3	8680
1-BJ-8	260	285	20.0	2340
1-BJ-9	406	281	13.8	3400
1-BJ-10	554	292	11.1	4370
1-BJ-11	722	293	9.1	5400
1-BJ-12	860	293	6.5	7520
1-BJ-16	290	300	14.5	3808
1-BJ-20	192	286	29.3	1642
1-BJ-24	287	297	13.8	3821
1-BJ-28	187	288	29.0	1665
1-BJ-32	105	278	52.6	749
1-BJ-36	104	277	47.9	896
1-BJ-40	186	289	31.2	1522
1-BJ-44	277	291	15.9	3421
1-BJ-48	277	294	17.2	3219
2-BJ-1	105	278	54.1	925
2-BJ-2	239	287	23.0	2607

TABLE A-2 (Cont'd)

Run	P_a Psi	T_m °F	ΔT °F	h Btu/hr sq ft °F
2-BJ-3	385	289	18.0	3515
2-BJ-4	538	293	13.3	4937
2-BJ-5	692	296	11.5	6013
2-BJ-6	834	296	9.8	7160
2-BJ-7	694	294	12.3	5663
2-BJ-11	690	278	15.1	4246
2-BJ-15	310	272	38.6	1349
1-BJ-56	281	280	21.9	2250
1-BJ-63	98	269	75.0	516
3-BJ-1	106	-236	48.8	163
3-BJ-2	203	-250	35.7	214
3-BJ-3	300	-257	23.0	371
3-BJ-4	303	-159	42.0	676
3-BJ-5	304	-33	58.7	987
3-BJ-15	102	-42	86.4	487
3-BJ-16	305	-53	45.8	1242
3-BJ-25	102	-33	78.1	537
3-BJ-26	305	-28	40.5	1353
4-BJ-1	101	-13	62.5	578
4-BJ-2	297	-25	28.5	1888
4-BJ-9	102	-20	69.4	512
4-BJ-16	298	-23	31.8	1665
4-BJ-17	99	281	27.6	1389
4-BJ-18	306	264	16.3	2910
4-BJ-29	98	267	43.8	770
4-BJ-30	99	274	44.4	857
4-BJ-31	305	265	15.4	3042

TABLE A-2(Cont'd)

Run	P_a Psi	T_m °F	ΔT °F	h Btu/hr sq ft °F
4-BJ-31	305	265	15.4	3042
4-BJ-39	96	264	53.2	710
4-BJ-40	99	287	34.9	1057
4-BJ-51	102	274	39.9	947
5-BJ-1	102	267	38.3	971
5-BJ-2	308	274	21.0	2286
5-BJ-6	102	279	27.1	1300
		Stainless Steel 304		
6-BJ-1	103	280	38.3	115
6-BJ-2	310	298	19.9	302
6-BJ-3	566	305	11.7	644
6-BJ-4	309	290	18.0	319
6-BJ-21	26	-59	118.3	16.5
6-BJ-22	91	-78	84.4	31.0
6-BJ-23	307	-88	46.5	74.6

TABLE A-3

TABULATED EXPERIMENTAL RESULTS

INTERSTITIAL MATERIALS

Run	P_a	T_m	ΔT	h	h_ℓ **
	Psi	°F	°F	Btu/hr sq ft °F	Btu/hr sq ft °F
			Silica Paper		
1-SI-13	112	199	266.3	5.76	---
1-SI-14	195	199	225.5	6.93	---
1-SI-15	289	200	223.1	9.74	---
3-SI-13	96	-113	395.9	2.40	---
3-SI-14	309	-114	386.8	5.95	---
4-SI-12	103	-109	391.0	2.01	3.07
4-SI-13	302	-109	381.7	6.11	6.19
4-SI-32	99	189	228.4	5.43	7.67
4-SI-33	309	185	212.7	14.1	15.2
			Asbestos Board		
1-AB-17	115	200	221.5	10.1	---
1-AB-18	209	200	219.5	11.2	---
1-AB-19	311	200	218.2	12.5	---
3-AB-6	127	-123	350.1	5.82	---
3-AB-7	301	-129	338.8	9.35	---
4-AB-7	107	-106	379.4	6.58	6.91
4-AB-8	303	-101	382.8	10.3	10.3
4-AB-21	100	189	212.0	12.9	13.1
4-AB-22	307	192	218.6	14.9	14.8
5-AB-3	310	194	235.8	15.0	14.4

** $h\ell$, Thermal contact resistance estimated from an energy loss calculation

TABLE A-3(Cont'd)

Run	P_a	T_m	ΔT	h	h_ℓ
	Psi	°F	°F	Btu/hr sq ft °F	Btu/hr sq ft °F
			Teflon		
1-TE-21	96	256	101.5	290	---
1-TE-22	201	260	92.5	344	---
1-TE-23	275	262	87.1	376	---
			Mica		
1-MI-25	101	218	184.9	51.4	---
1-MI-26	187	226	160.7	93.9	---
1-MI-27	275	233	149.1	121	---
4-MIB-35	99	199	197.8	29.9	31.1
4-MIB-36	209	206	191.2	49.8	50.6
4-MIB-37	313	210	178.4	69.9	68.1
4-MIG-38	97	210	200.9	42.5	41.0
4-MIG-41	99	205	184.1	49.3	41.2
5-MIC-5	309	211	183.7	59.6	57.9
6-MIC5-15	107	216	177.1	9.09	---
6-MIC5-16	312	227	148.2	16.8	---
6-MIC-17	25	252	116.5	21.9	---
6-MIC-18	57	253	114.3	26.0	---
6-MIC-19	106	253	105.9	32.3	---
6-MIC-20	309	268	72.3	65.5	---
6-MIC-24	28	-6.3	149.4	19.1	---
6-MIC-25	100	-9.5	104.1	35.7	---
6-MIC-26	301	-7.1	72.0	70.1	---
			Asbestos Tape		
1-AT-29	102	204	215.5	15.7	---
1-AT-30	189	204	212.	16.8	---

TABLE A-3(Cont'd)

Run	P_a	T_m	ΔT	h	h_ℓ
	Psi	°F	°F	Btu/hr sq ft °F	Btu/hr sq ft °F
1-AT-31	281	205	212.0	19.7	---
3-AT-8	114	-139	308.2	11.0	---
3-AT-9	231	-137	315.0	13.0	---
4-AT-43	104	189	22.7	21.4	18.8
			Carbon Paper		
1-CA-33	101	196	222.0	4.84	---
1-CA-34	188	197	220.6	6.78	---
1-CA-35	276	198	219.8	8.74	---
3-CA-19	102	-103	418.9	1.50	---
3-CA-20	299	-106	410.3	2.76	---
4-CA-10	104	-103	419.3	1.11	1.82
4-CA-11	296	-112	399.5	3.16	3.76
4-CA-25	95	188	228.4	4.04	3.71
4-CA-26	305	188	219.1	8.48	8.47
5-CA-4	307	191	219.4	9.52	10.8
6-CA6-9	112	192	239.0	0.89	---
6-CA6-10	313	193	232.6	1.80	---
6-CA-11	28	202	227.1	2.15	---
6-CA-12	60	202	219.2	2.83	---
6-CA-13	108	204	191.7	5.85	---
6-CA-14	315	211	162.3	11.2	---
6-CA-27	28	-58	376.8	1.41	---
6-CA-28	104	-63	354.8	2.55	---
6-CA-29	302	-65	281.9	5.79	---
			Ceramic Paper		
1-CE-37	102	199	230.8	3.82	---
1-CE-38	188	198	227.1	4.73	---

TABLE A-3(Cont'd)

Run	P_a	T_m	ΔT	h	h_ℓ
	Psi	°F	°F	Btu/hr sq ft °F	Btu/hr sq ft °F
1-CE-39	279	199	225.5	6.22	---
4-CE-14	101	-111	395.7	1.30	2.29
4-CE-15	296	-111	397.4	2.26	3.04
4-CE-27	99	191	232.1	3.95	1.93
4-CE-28	301	193	233.9	7.86	5.72
			Laminate T-30LR		
1-LA-41	104	197	224.5	3.21	---
1-LA-42	182	198	225.5	3.13	---
1-LA-43	278	197	225.2	3.33	---
3-LA-10	119	-116	395.4	1.10*	---
3-LA-11	305	-117	395.3	1.50*	---
3-LA-12	109	-87	455.3	0.56	---
4-LA-3	102	-108	403.3	0.62*	1.58
4-LA-4	306	-111	405.1	1.14*	2.13
4-LA-23	102	193	213.7	2.13	2.11
4-LA-24	307	188	213.8	3.29	2.48
			Pluton B-1 Cloth		
1-PL-45	105	192	236.4	18.4	---
1-PL-46	188	193	228.9	23.7	---
1-PL-47	279	196	225.6	28.2	---
3-PL-17	104	-119	356.5	6.57	---
3-PL18	305	-118	350.5	11.6	---
4-PL-34	101	197	210.2	18.8	25.2
			WRP-X-AQ Felt		
1-FE-49	106	183	255.6	1.48	---
1-FE-50	188	184	255.7	1.15	---

* Estimated by Δ1/2°F deviation

TABLE A-3(Cont'd)

Run	P_a	T_m	ΔT	h	h_ℓ
	Psi	°F	°F	Btu/hr sq ft °F	Btu/hr sq ft °F
1-FE-51	280	183	253.8	1.61	---
4-FE-5	107	-113	405.0	1.14*	0.60
4-FE-6	305	-114	399.2	1.12*	1.02
4-FE-19	106	187	238.3	0.99	0.73
4-FE-20	310	187	238.3	1.84	1.50
4-FE-44	103	185	247.9	0.54	0.36
4-FE-45	308	185	242.8	2.43	1.83
4-FE-46	561	185	239.8	3.40	3.32
4-FE-47	806	181	232.8	4.22	4.88
4-FE-48	1006	179	228.1	6.28	6.10
4-FE-49	562	178	230.4	5.11	5.31
4-FE-50	115	193	263.3	2.0	2.19
6-FE-5	27	196	229.1	0.82	---
6-FE-6	49	194	232.3	0.95	---
6-FE-7	108	193	233.1	1.02	---
6-FE-8	312	195	225.0	2.02	---
			Pyroid Disk		
1-PY-52	109	217	174.4	96	---
1-PY-53	187	221	172.1	102	---
1-PY-54	277	219	169.2	107	---
			Zirconium Disk		
2-ZI-8	107	182	248.2	4.08	---
2-ZI-9	187	182	249.0	5.13	---
2-ZI-10	276	183	249.5	6.06	---
4-ZI-42	107	190	232.7	5.46	3.75

*Estimated by Δ1/2°F deviation

TABLE A-3(Cont'd)

Run	P_a	T_m	ΔT	h	h_ℓ
	Psi	°F	°F	Btu/hr sq ft °F	Btu/hr sq ft °F
Magnesium Disk					
2-MA-12	134	209	222.9	45.5	---
2-MA-13	209	208	186.9	80.3	---
2-MA-14	308	212	164.6	121.5	---
Stainless Steel Screen--10 Mesh					
2-SS10-16	132	192	239.8	17.3	---
2-SS10-17	192	190	231.4	19.5	---
2-SS10-18	279	191	229.0	23.9	---
3-SS10-23	104	-106	378.2	7.40	---
3-SS10-24	299	-104	374.6	12.7	---
Stainless Steel Screen--100 Mesh					
1-SS100-57	96	216	183.0	64.6	---
1-SS100-58	187	220	167.6	90.1	---
1-SS100-59	277	229	157.2	118	---
Titanium Screen--10 Mesh					
1-TI10-60	102	195	231.9	10.7	---
1-TI10-61	186	192	233.6	16.3	---
1-TI10-62	275	189	218.9	21.9	---
Tungsten Screen--20 Mesh					
1-W20-64	99	218	143.4	118	---
1-W20-65	186	229	136.3	152	---
1-W20-66	278	246	135.0	186	---

*Estimated by Δ1/2 °F deviation

APPENDIX B

UNCERTAINTY ANALYSIS

The junction thermal conductance is defined as

$$h = \frac{q}{\Delta T}$$

where q is determined from the product of the thermal conductivity and temperature gradient in the metal test specimen. The calculation of q by an energy balance method for the very low heat flux runs with aluminum specimens is discussed on page 31. Since q/A is evaluated as the product of two terms, the uncertainty as a percentage is given by

$$\frac{\delta(q)}{q} = \left\{ \left[\frac{\delta k}{k} \right]^2 + \left[\frac{\delta(dt/dx)}{dt/dx} \right]^2 \right\}^{1/2}$$

As an estimate of the uncertainty in the published thermal conductivity values and graphical interpolation (Figure 9) a value of 5 percent was selected. For each run a maximum and minimum slope (dt/dx) was read from the plot of specimen temperature versus length. In all cases the slope variation was well within ±1°F/inch. From these results a reasonable estimate of the uncertainty in dt/dx is 0.5°F/inch for the low heat flux runs with interstitial materials and perhaps as large as 1 1/2°F/inch for the much greater heat flux tests with the bare junction. All high temperature runs were conducted with water as the coolant and for the interstitial materials the mean temperature varied somewhat with the heat flux. Therefore, the magnitudes

of $\delta q/q$, the estimated uncertainty in the calculated heat flux is presented as a function of Q_j in Figure 16. Maximum and minimum possible slopes (dt/dx) were also estimated from the graphs of temperature versus length. The magnitudes of $\delta q/q$ calculated from these limiting slopes are also plotted in Figure 16. By comparison, the estimated uncertainties in dt/dx and k seem valid. The maximum Q_j value plotted is 101 Btu/hr which corresponds to the 100 mesh stainless steel screen run at 300 psi. The same plot for the stainless steel specimens would indicate somewhat lower uncertainties since for a given heat flux, dt/dx would be approximately 10 times larger for the stainless steel than for the aluminum specimens.

For the interstitial material runs it would be possible to have an error of as much as 4°F in the value for ΔT, the junction temperature difference. However, from the test results it was estimated that the uncertainty would be between 2°F and 4°F. For the high temperature tests with the aluminum specimens the junction temperature difference was approximately 200°F, and for the low temperature runs (liquid nitrogen coolant) the value of ΔT was between 300°F and 400°F. Therefore, the maximum percent uncertainty for ΔT occurred during the high temperature runs and was on the order of 2 percent. For stainless steel specimens ΔT was as small as 100°F so that the percent uncertainty, $\delta \Delta T/T$, is increased to 4 percent.

The estimated uncertainties in ΔT and q can be combined to calculate the uncertainty in h,

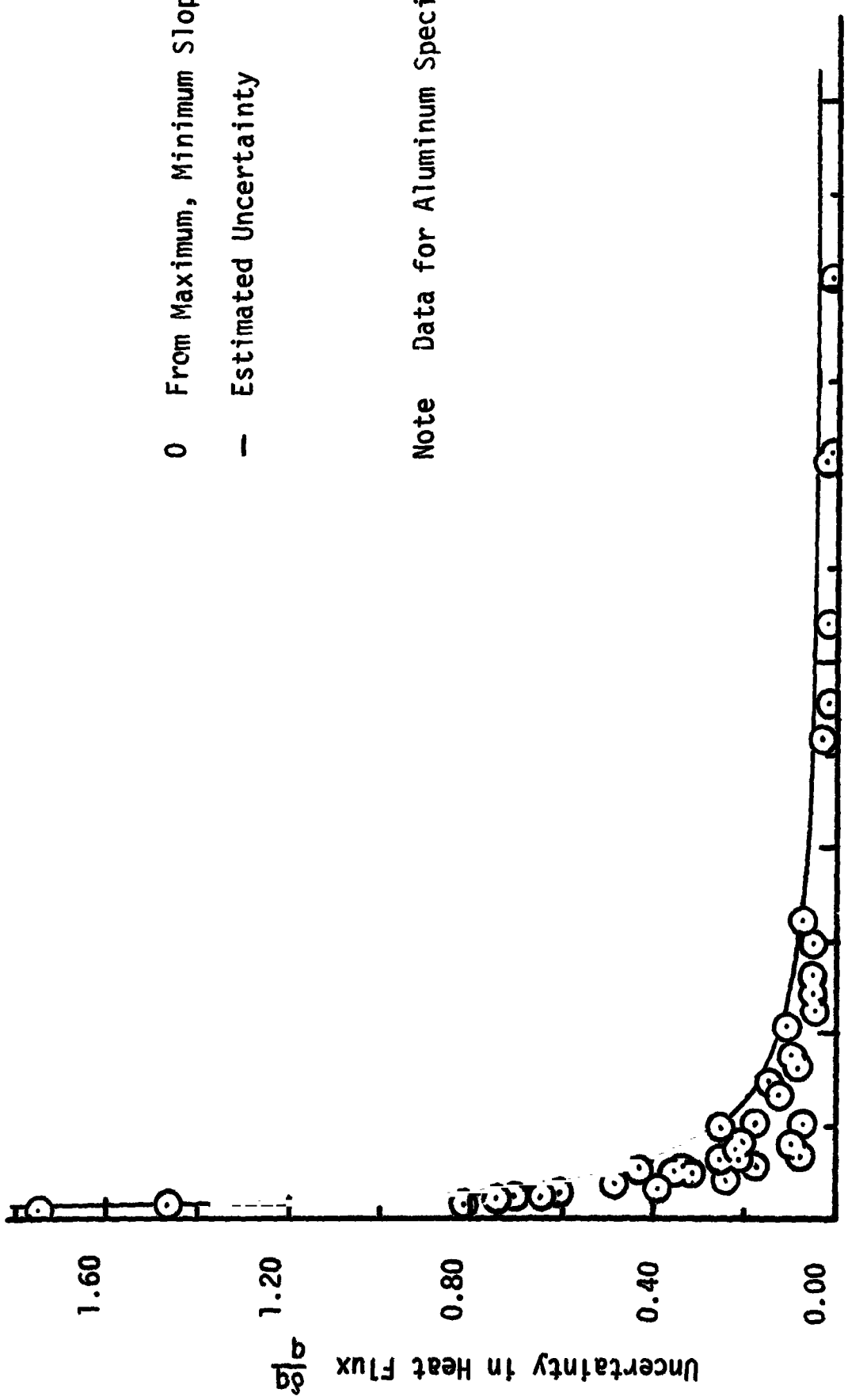

FIGURE 16. Estimated Uncertainty in Heat Flux

$$(\delta h/h) = \{ (\frac{\delta q}{q})^2 + (\frac{\delta \Delta T}{\Delta T})^2 \}^{1/2}$$

Since the magnitude varies with q, hence h, the ratio $\delta h/h$ is presented graphically as a function of h in Figure 17.

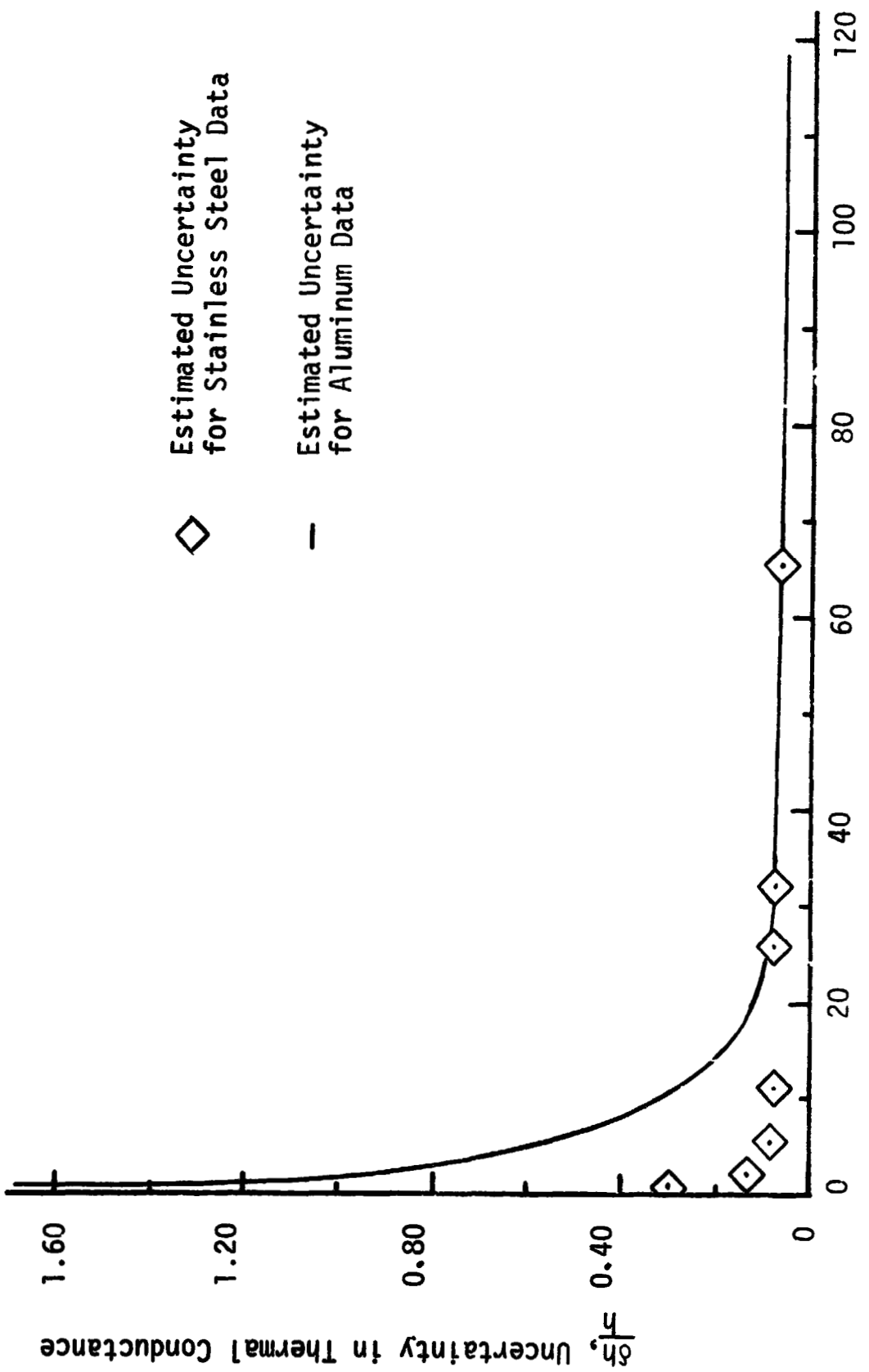

FIGURE 17. Estimated Uncertainty in Thermal Conductance